

Structure and lifetime in ionic liquids and their mixtures

Supporting Information

Sascha Gehrke^{a,b}, Michael von Domaros^a, Ryan Clark^d, Oldamur Hollóczki^a, Martin Brehm^c, Tom Welton,^d Alenka Luzar^e and Barbara Kirchner^{*a}

July 10, 2017

^a Mulliken Center for Theoretical Chemistry, University of Bonn, Beringstr. 4+6, D-53115 Bonn, Germany.

E-mail: kirchner@thch.uni-bonn.de

^b Max Planck Institute for Chemical Energy Conversion, Stiftstr. 34-36, D-45413 Mülheim an der Ruhr, Germany

^c Theoretical Chemistry, Martin-Luther-University Halle-Wittenberg, Universitätsplatz 10, D-06108 Halle

^d Imperial College London, South Kensington Campus, London SW7 2AZ, UK

^e Department of Chemistry, Virginia Commonwealth University, Richmond, Virginia 23284-2006, United States

Contents

1 Computational Details	3
1.1 Molecular Dynamics Simulations	3
1.2 Analysis and Data Handling	4
1.3 Technical Details of the Reactive Flux Analysis	5
2 Results: Structure	6
2.1 RDFs	6
2.1.1 [C ₄ C ₁ Im][Br]	6
2.1.2 Temperature Dependency	7
2.1.3 Mixture of IL with Water	13
2.1.4 Ionic Liquid Mixtures	17
2.2 CDFs	20
2.2.1 [C ₄ C ₁ Im][Br]	20
2.2.2 Temperature Dependency	22
2.2.3 Mixture of IL with Water	27
2.2.4 Ionic Liquid Mixtures	39
3 Results: Dynamics	45
3.1 Reactive Flux Functions	45
3.2 Mixtures of IL and Water	47
3.3 Ionic Liquid Mixtures	49
4 Results: Correlating Viscosity with Ion Pair Dynamics	51
4.1 Experimental and Calculated Viscosities	51
5 Experimental Setup	52
5.1 Mixture Synthesis	52
5.2 NMR Measurements	53
5.3 Diffusion Summary	53
5.3.1 Temperature dependence	53
5.3.2 Ionic liquid mixtures	54
5.4 Detailed Diffusion Results	55
5.4.1 Temperature dependence	55
5.4.2 Ionic liquid mixtures	57

1 Computational Details

1.1 Molecular Dynamics Simulations

The simulated systems were modeled by using the OPLS force field¹, which was extended by the parameter set for the imidazolium ring unit developed by Canongia Lopez and Padua.² The parameters for the halides were taken from the same work.² The applied parameters for the triflate anions were taken from a previous publication of the same group.³ This family of force fields has shown a good representation of the mass transport properties if the ionic charges were scaled by a factor of 0.8. Thus, we scaled the charges of all cations and anions.

Another way to simulate ionic liquids with classical MD is the application of a polarizable force field such as the drude model. The charges were split into two different point charges, one on the atomic core, the other one connected to the core by a strong harmonic potential.⁴ The distribution of the charges between the two point charges was chosen to represent the atomic polarizabilities.^{5,6} Finally, the water molecules in the mixtures containing water were described by the SPC/E water model.⁷

To obtain Lennard-Jones cross terms, especially for the interactions between the different force fields, Lorentz–Berthelot mixing rules^{8,9} ($\epsilon_{ij} = \sqrt{\epsilon_i \epsilon_j}$ and $\sigma_{ij} = \frac{1}{2}(\sigma_i + \sigma_j)$) were applied. Non-bonded interactions were computed only if the distance between the involved atoms was within a cutoff radius of 10 Å. Coulombic interactions beyond this distance were computed via the particle–particle particle–mesh solver¹⁰ with an accuracy of 10^{-5} .

All the simulations were carried out by the LAMMPS software package¹¹ according to the following protocol:

1. The initial configuration of each cell with a composition as summarized in Tab. 1 was generated applying PACKMOL¹², with a density chosen as equivalent to the respective experimental value. Possible hotspots in these configuration were removed by minimizing the energy of the geometry.
2. The system was simulated in an *NVT* ensemble for 0.5 ns. The timestep for the integration of the Newton equations was chosen to be 1.0 fs. The temperature was controlled by a Nosé–Hoover chain thermostat ($\tau = 100$ fs).
3. The system was then simulated for 1.0 ns in an *NpT* ensemble to relax the cells to the optimal density of the applied force fields. Constant pressure and temperature were provided by applying a Nosé–Hoover chain thermostat ($\tau = 100$ fs) and a Nosé–Hoover barostat ($p = 1$ bar, $\tau = 1000$ fs), respectively.^{13–15} Over the last 0.5 ns the box volume was averaged.
4. The system was mildly forced to the obtained average volume over 0.1 ns. Finally, the ensemble was switched back to *NVT*, assuring a constant temperature again by Nosé–Hoover chain thermostat ($\tau = 100$ fs). The final density during the simulations are summarized in Tab. 2.

- After an equilibration period of 5.0 ns, the production runs were performed for 10.0 ns, storing the coordinates of the systems every 1 ps. For the last 200 ps the snapshots were stored every 1 fs, to get a sufficient resolution in the analysis of the non-covalent dynamics.

Table 1: Compositions of the investigated systems.

pure [C ₄ C ₁ Im][Br]			
Model	[C ₄ C ₁ Im]	[Br]	
ff	500	500	
pol-ff	500	500	
Temperature dependent [C ₄ C ₁ Im][OTf]			
T in K	[C ₄ C ₁ Im]	[OTf]	
293	300	300	
323	300	300	
353	300	300	
373	300	300	
393	300	300	
[C ₄ C ₁ Im][OTf]/water mixtures			
x of IL	[C ₄ C ₁ Im]	[OTf]	H ₂ O
0.39	197	197	303
0.58	288	288	212
0.66	330	330	170
0.82	410	410	90
[C ₄ C ₁ Im][OTf]/[Cl] mixtures			
x of [Cl]	[C ₄ C ₁ Im]	[OTf]	[Cl]
0.000	300	300	—
0.192	500	404	96
0.303	501	349	152
0.402	500	299	201

1.2 Analysis and Data Handling

Our open source program TRAVIS (Trajectory Analyzer and Visualizer) was used to examine the trajectories of the simulated systems.²⁰ The most used structural analyses are radial distribution functions (RDFs) and combined distribution functions (CDFs), which are visualized with the aid of the program gnuplot (version 4.6)²¹ for the generation of three-dimensional plots of data or with the xmGrace software²². In addition, we used the partly newly implemented function of the hydrogen bond (HB), the ion pair (IP) and the ion cage (IC) time correlation functions.

Table 2: Densities of the simulated systems in g cm⁻³.

		calc.	exp.
[C ₄ C ₁ Im][Br]	ff	1.1409	
	pol-ff	0.9803	
[C ₄ C ₁ Im][OTf]	293 K	1.2893	1.3061 (293 K) ¹⁶ 1.3097 (293 K) ¹⁷
	323 K	1.2546	1.2787 (323 K) ¹⁶ 1.2848 (323 K) ¹⁷ 1.2844 (323 K) ¹⁸
	353 K	1.2296	1.2540 (353 K) ¹⁶ 1.2618 (353 K) ¹⁷
	373 K	1.2087	1.2396 (373 K) ¹⁶
	393 K	1.1948	1.2253 (393 K) ¹⁶
[C ₄ C ₁ Im][Br]/H ₂ O	0.39	1.2603	1.2630 (0.4077, 303.15 K) ¹⁸
	0.58	1.2704	1.2808 (0.6001, 303.15 K) ¹⁸
	0.66	1.2783	1.2865 (0.7013, 303.15 K) ¹⁸
	0.82	1.2823	1.2912 (0.8061, 303.15 K) ¹⁸
[C ₄ C ₁ Im][OTf]/[Cl]	0.000	1.2790	1.2896 (298.15 K) ¹⁹
	0.192	1.2165	1.2585 (298.15 K) ¹⁹
	0.303	1.2119	1.2384 (298.15 K) ¹⁹
	0.402	1.1935	1.2192 (298.15 K) ¹⁹

1.3 Technical Details of the Reactive Flux Analysis

The analysis of the reactive flux dynamics is done in three steps: step-by-step processing of the trajectory, correlating of the collected state functions and finally fitting of the data to the Luzar–Chandler model.

During the processing all pairs of anion and cation which are fulfilling the previously defined criteria for neighborhood on the one hand, and pairing or bonding on the other hand are identified. The neighboring criterion is defined by a cut-off distance between two certain atoms which is obtained from the first minimum in the corresponding RDFs. We can safely do this without a loss in accuracy, since the resolution of our RDFs is good enough for this purpose. The influence of varying the cutoff distance by 1, 5, 10 pm which is within the uncertainty of our RDFs was tested and found to be insignificant. The criterion for hydrogen bonds consists of a distance between hydrogen atom and acceptor atom, obtained from the corresponding RDFs, and the angle between donor–hydrogen–acceptor, which was chosen for all systems to be greater than 120 degrees. This decision is justified by the well-defined occurrence in the corresponding CDFs (Figs. 14 to 38). For the ion pairs we defined a cation and an anion as a pair if they are nearest neighbors. If one or both of these states has changed compared to the previous step the current step number is saved for each involved pair.

After the processing is finished, the two functions — one for the pairing or bonding, one for the neighboring — are restored as arrays of zeroes and ones and Fourier transformed for every certain pair of cation and anion. In the Fourier space two new functions are obtained by multiplying the ion pair function with itself and with the neighboring function, respectively. The obtained result functions are transformed back into normal space. The Fourier transformation scheme is applied to speed up the calculation of the autocor-

relation function of the pairing and the cross-correlation function of the pairing and the neighboring, following the Wiener-Khinchin theorem^{23,24} and the cross-correlation theorem. After normalization the first result function is equal to the autocorrelation function $c(t)$ (see Theory section in the article). From this function $c(t)$ the normalized second result function — the cross-correlation function of the pairing and the neighboring — is subtracted to obtain the function $n(t)$. At last the derivative $k(t)$ of $c(t)$ is calculated numerically.

Finally, a simplified steepest descent algorithm is applied to find two parameters k_f and k_b in a way that the root mean square displacement to Equation 6 in the main article is minimized. The given lifetimes in the article are obtained from the inverse k_f and k_b parameters. The rate constant k_{TST} is obtained from the first value of the derivative function $k(t)$.

2 Results: Structure

2.1 RDFs

2.1.1 [C₄C₁Im][Br]

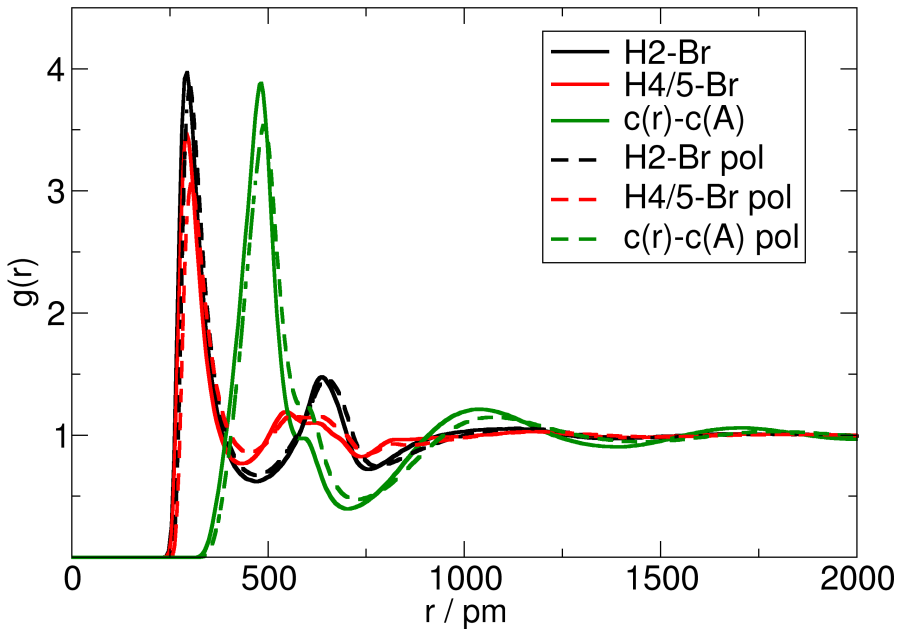


Figure 1: Full radial distribution functions (RDFs) of the pure [C₄C₁Im][Br] systems (compare Fig. 2 in the main article).

2.1.2 Temperature Dependency

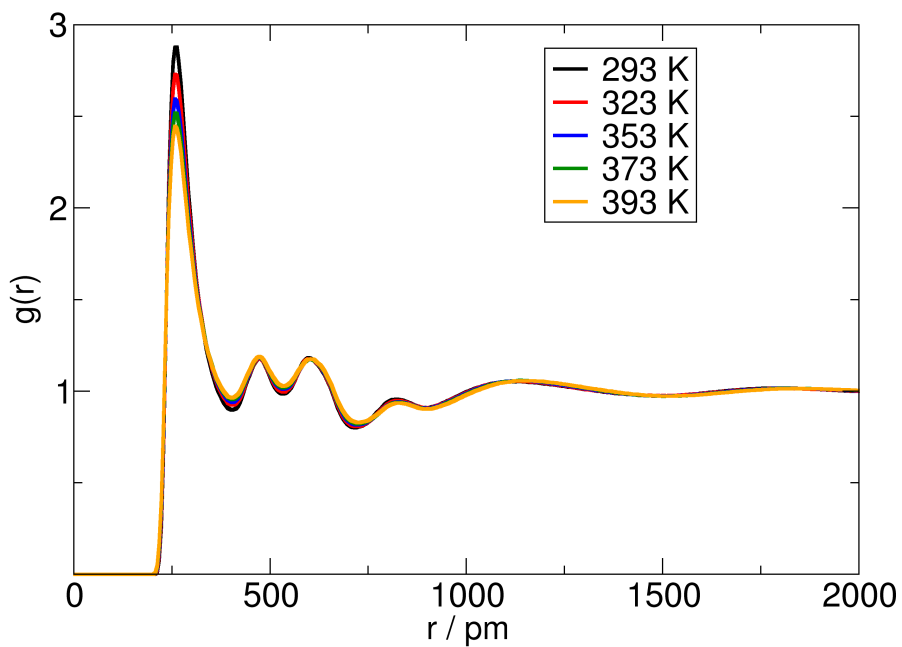


Figure 2: Full radial distribution functions (RDFs) between the H₂ of the cation and the O of the anions in the pure [C₄C₁Im][OTf] systems. For an enlarged illustration of the first peaks see Fig. 5.

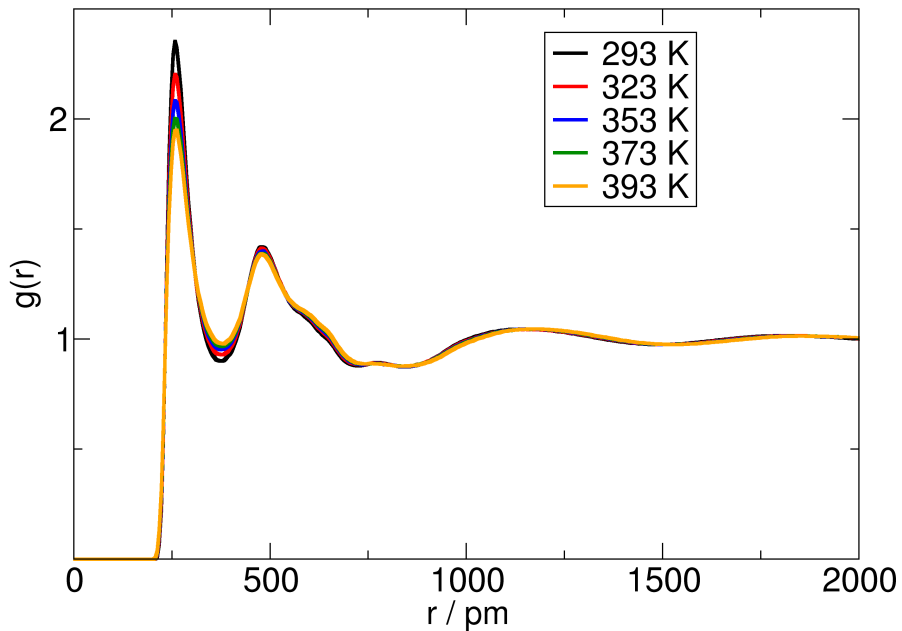


Figure 3: Full radial distribution functions (RDFs) between the H4 and the H5 of the cation and the O of the anions in the pure $[\text{C}_4\text{C}_1\text{Im}][\text{OTf}]$ systems. For an enlarged illustration of the first peaks see Fig. 6.

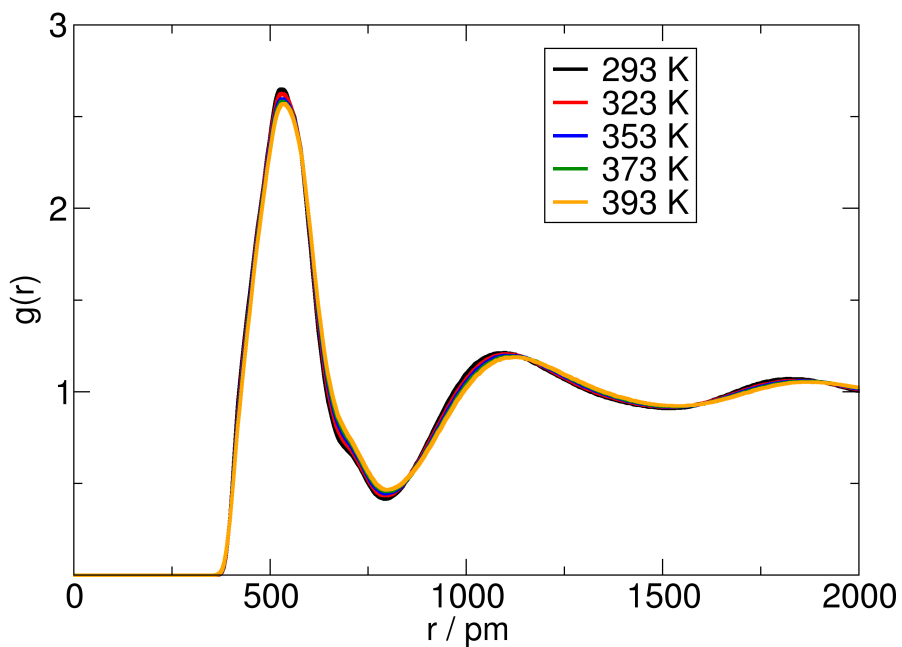


Figure 4: Full radial distribution functions (RDFs) between the center of the ring of the cation and the center of mass of the anions in the pure $[C_4C_1Im][OTf]$ systems. For an enlarged illustration of the first peaks see Fig. 7.

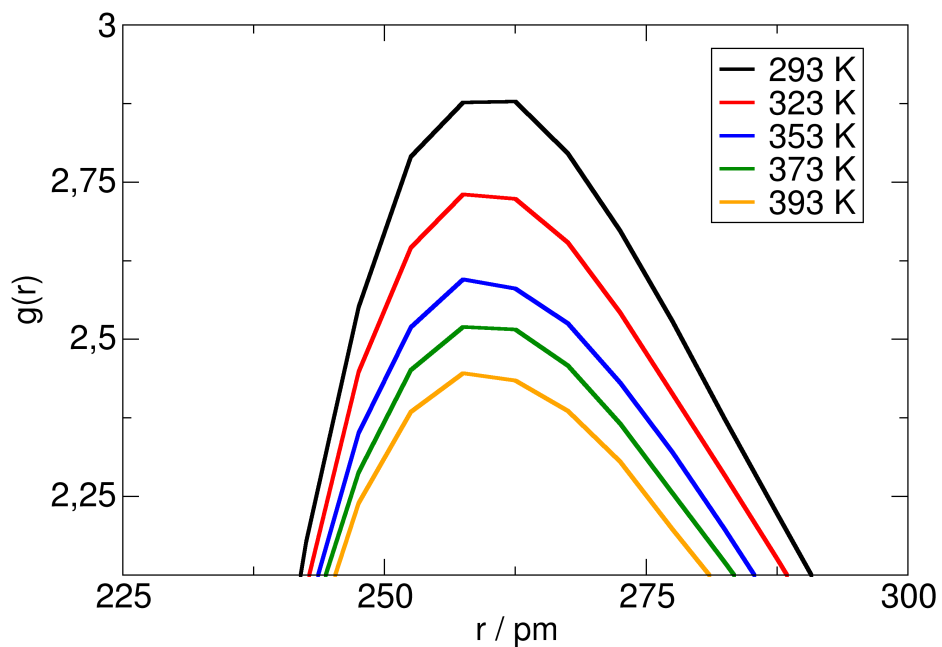


Figure 5: Magnified first peaks of the radial distribution functions (RDFs) between the H₂ of the cation and the O of the anions in the pure [C₄C₁Im][OTf] systems.

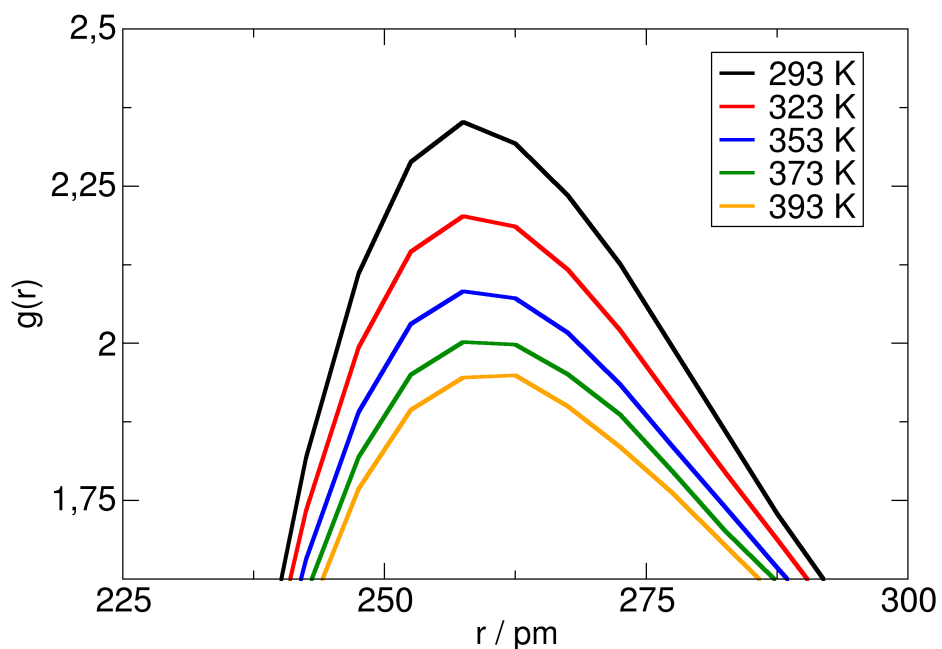


Figure 6: Magnified first peaks of the radial distribution functions (RDFs) between the H4 and the H5 of the cation and the O of the anions in the pure [C₄C₁Im][OTf] systems.

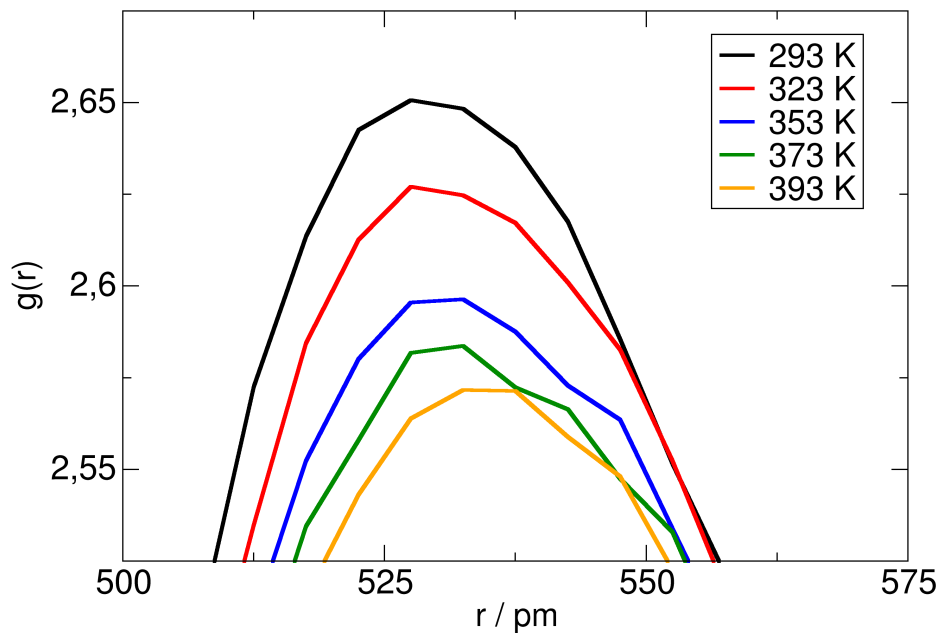


Figure 7: Magnified first peaks of the radial distribution functions (RDFs) between the center of the ring of the cation and the center of mass of the anions in the pure $[C_4C_1Im][OTf]$ systems.

2.1.3 Mixture of IL with Water

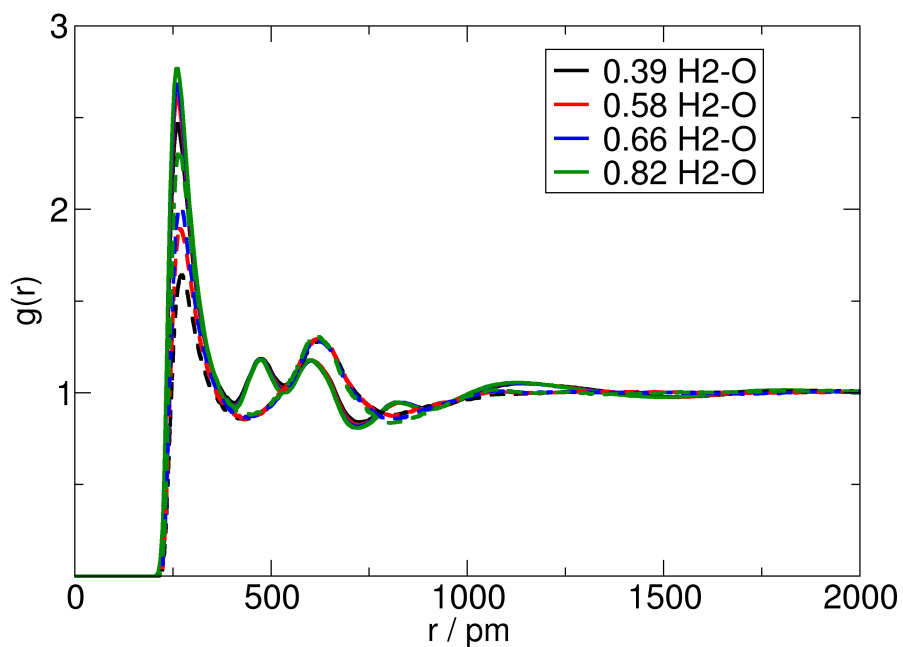


Figure 8: Full radial distribution functions (RDFs) of the $[C_4C_1Im][OTf]$ /water mixtures.
Solid line: H₂(cation) - O (OTf); Dashed line: H₂(cation) - O (water)

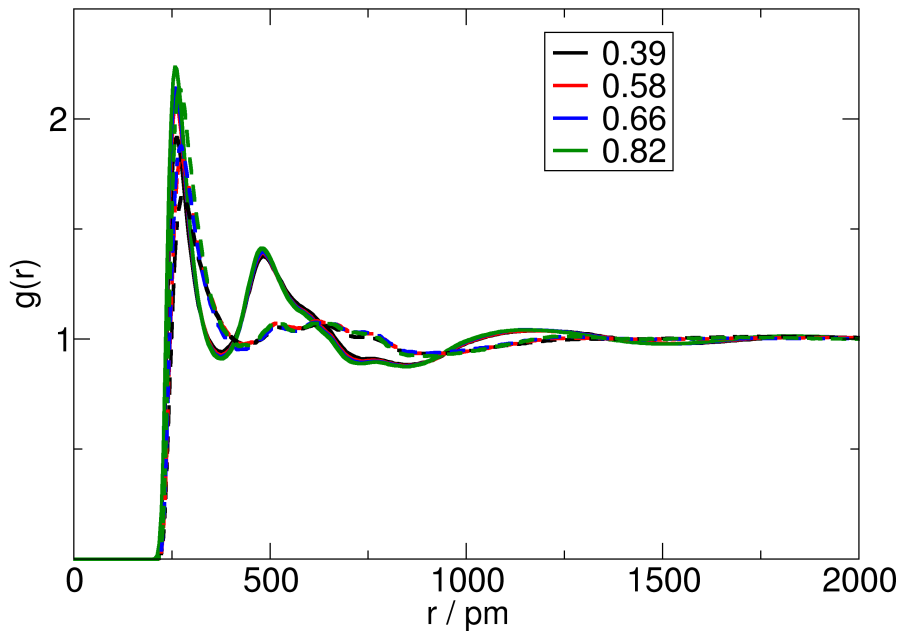


Figure 9: Full radial distribution functions (RDFs) of the $[C_4C_1Im][OTf]$ /water mixtures.
Solid line: H45(cation) - O (OTf); Dashed line: H45(cation) - O (water)

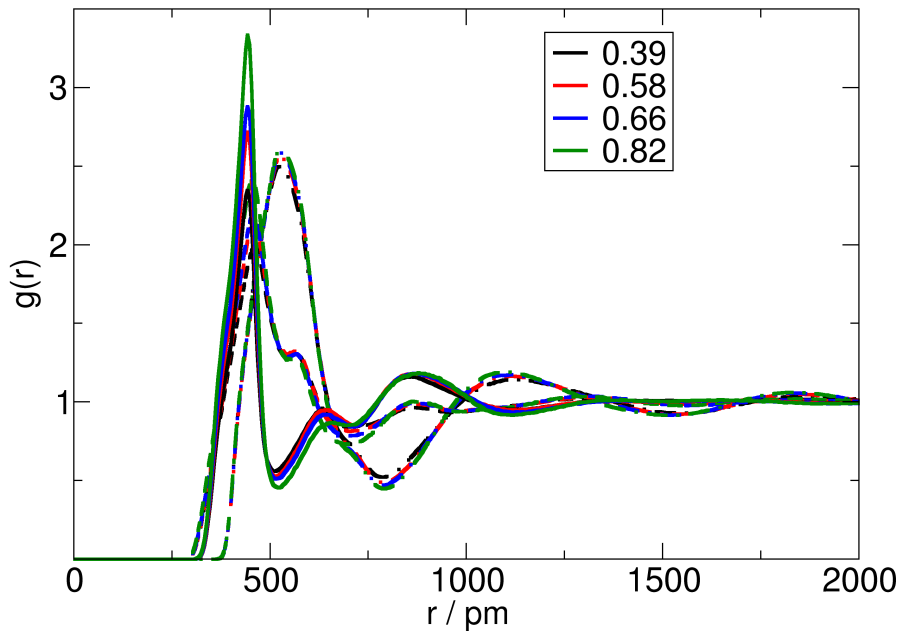


Figure 10: Full radial distribution functions (RDFs) of the $[C_4C_1Im][OTf]$ /water mixtures (compare Fig. 4 in the main article). Dashed-dotted: $c(R)-c(A)$; Solid line: $c(A)-c(W)$; Dashed line: $c(R)-c(W)$

Table 3: Distance of first maximum $r(\max)$, first minimum $r(\min)$, NI and \bar{NI} in $[C_4C_1Im][OTf]/water$ for H₂-O and H₄/5-O as well as for center of ring ($c(r)$) and mass of anion ($c(A)$) and water ($c(w)$) in order to compare “interaction strength“ for different mole fractions. Temperature = 293 K. x gives the mole fraction of the IL.

x	H ₂ -O(IL)	H ₂ -O(w)	H(w)-O(IL)
r(max)/r(min)/NI/NI			
0.39	263/408/2.4/0.8	273/433/1.1/0.7	178/253/0.5/0.5
0.58	263/403/2.5/0.8	268/438/0.6/0.9	178/258/0.6/0.3
0.66	263/408/2.6/0.9	268/433/0.5/0.9	178/258/0.7/0.2
0.82	263/408/2.7/0.9	268/428/0.2/0.9	178/258/0.8/0.1
x	H ₄ /5-O(IL)	H ₄ /5-O(w)	H(w)-O(w)
r(max)/r(min)/NI/NI			
0.39	263/378/1.6/1.1	278/433/1.3/1.6	173/243/3.0/1.5
0.58	263/373/1.7/1.1	273/428/0.6/1.7	178/248/2.8/1.4
0.66	258/373/1.7/1.2	273/418/0.4/1.6	173/248/2.6/1.3
0.82	258/378/1.9/1.2	268/423/0.2/1.8	178/248/2.4/1.2

2.1.4 Ionic Liquid Mixtures

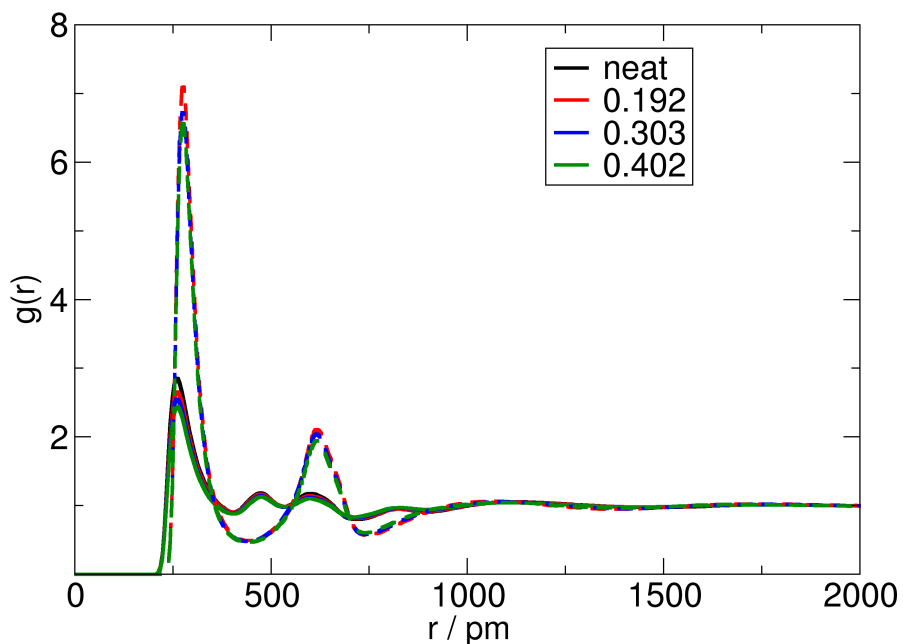


Figure 11: Full radial distribution functions (RDFs) between the H₂ atom of the cation and the anion of the [C₄C₁Im][OTf]/[Cl] mixtures (compare Fig. 5 in the main article). Solid line: H₂-O; Dashed line: H₂-Cl

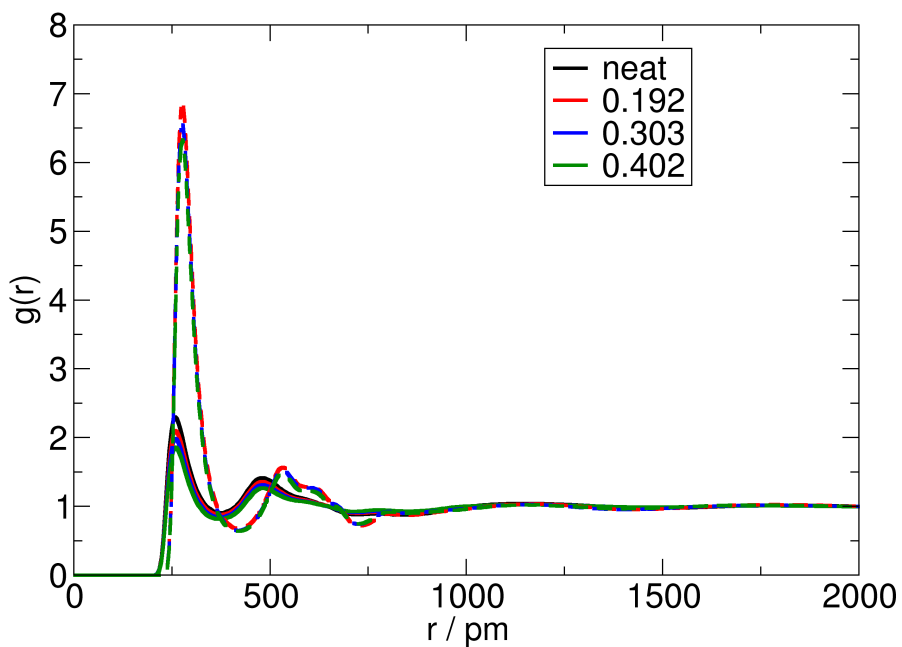


Figure 12: Full radial distribution functions (RDFs) between the H4 and H5 atom of the cation and the anion of the $[C_4C_1Im][OTf]/[Cl]$ mixtures. Solid line: H45-O; Dashed line: H45-Cl

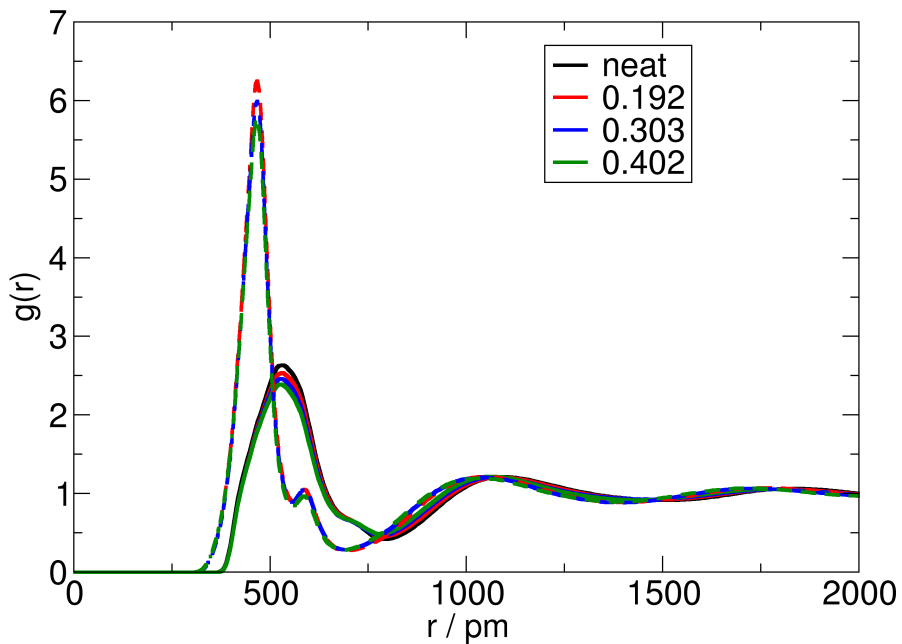


Figure 13: Full radial distribution functions (RDFs) between the center of ring of the cations and the center of mass of the respective anion of the $[C_4C_1Im][OTf]/[Cl]$ mixtures (compare Fig. 4 in the main article). Solid line: $c(R)-c(OTf)$; Dashed line: $c(R)-c(Cl)$

2.2 CDFs

2.2.1 $[C_4C_1Im][Br]$

$[C_4C_1Im][Br]$ – non-polarizable force field

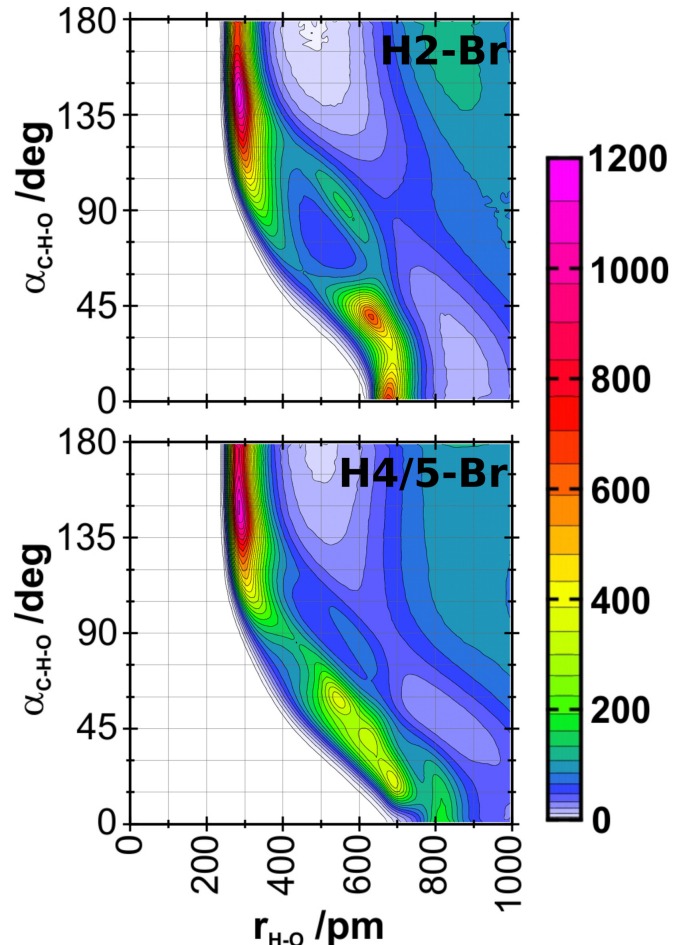


Figure 14: CDFs for occurring HB geometries in $[C_4C_1Im][Br]$ simulated with the non-polarizable force field. Donor-hydrogen-acceptor angle vs. acceptor-hydrogen distance is shown. In the upper panel the interplay between H2 and Br is illustrated, in the lower the interplay between H4, H5 and Br.

[C₄C₁Im][Br] – polarizable force field

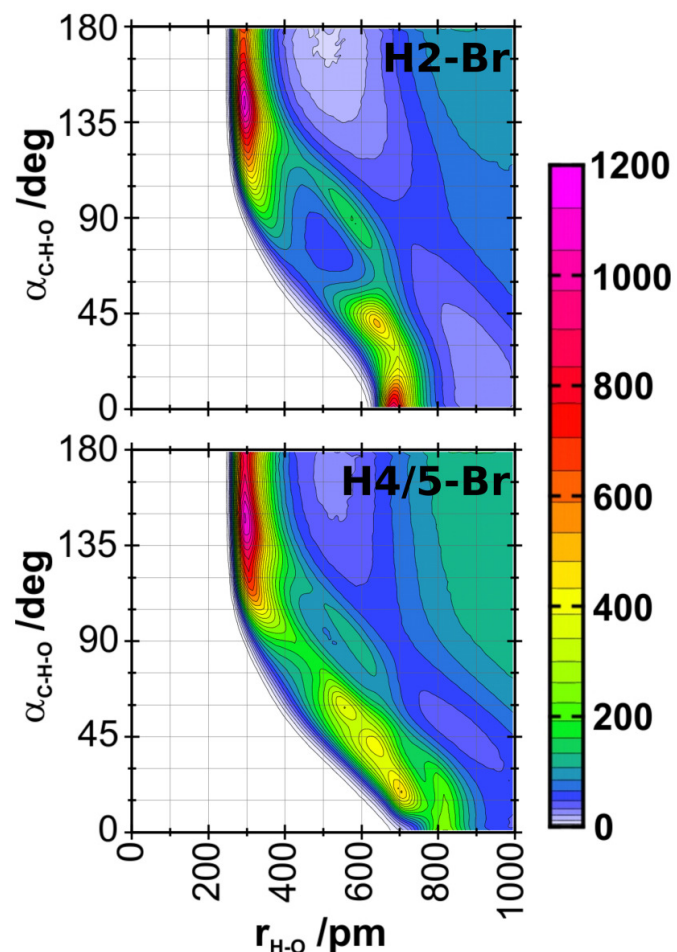


Figure 15: CDFs for occurring HB geometries in [C₄C₁Im][Br] simulated with the polarizable force field. Donor-hydrogen-acceptor angle vs. acceptor-hydrogen distance is shown. In the upper panel the interplay between H2 and Br is illustrated, in the lower the interplay between H4, H5 and Br.

2.2.2 Temperature Dependency

[C₄C₁Im][OTf] at 293 K

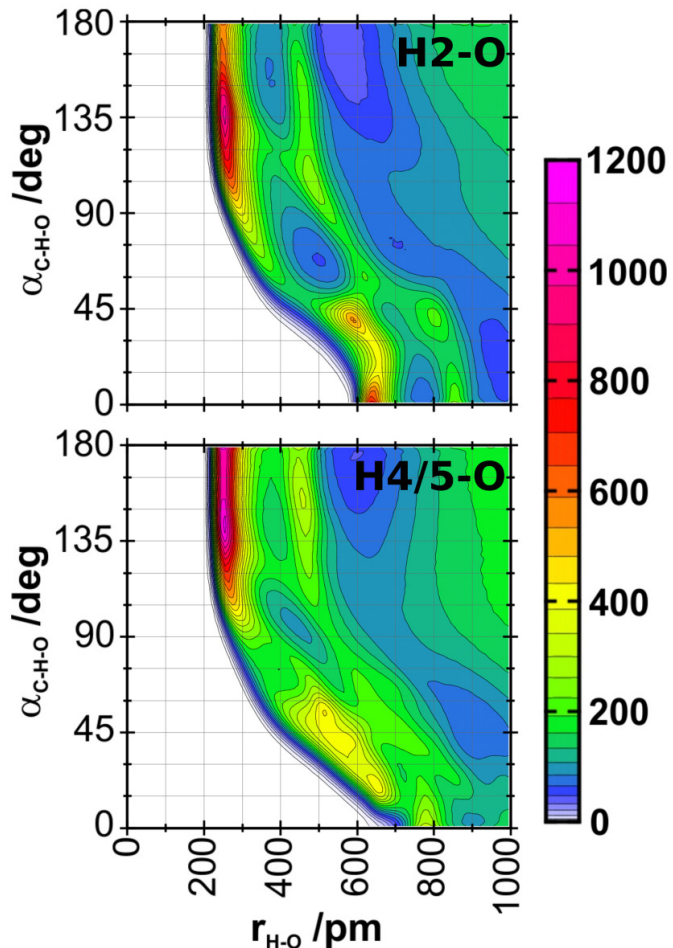


Figure 16: CDFs for occurring HB geometries in [C₄C₁Im][OTf] simulated at 293 K. Donor-hydrogen-acceptor angle vs. acceptor-hydrogen distance is shown. In the upper panel the interplay between H2 and the O atoms is illustrated, in the lower the interplay between H4, H5 and the O atoms.

$[C_4C_1Im][OTf]$ at 323 K

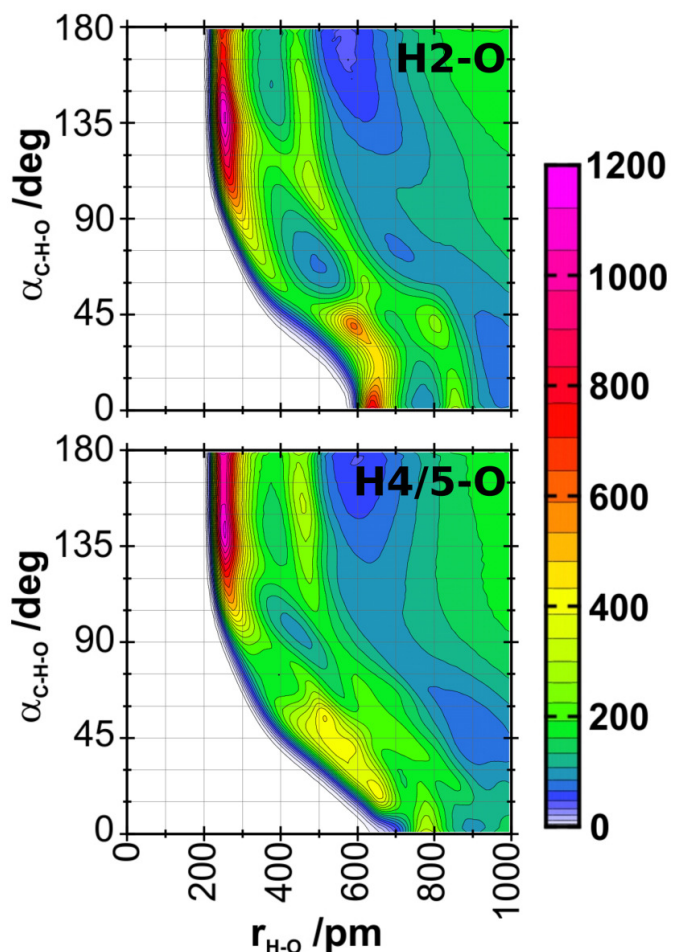


Figure 17: CDFs for occurring HB geometries in $[C_4C_1Im][OTf]$ simulated at 323 K. Donor-hydrogen-acceptor angle vs. acceptor-hydrogen distance is shown. In the upper panel the interplay between H2 and the O atoms is illustrated, in the lower the interplay between H4, H5 and the O atoms.

$[C_4C_1Im][OTf]$ at 353 K

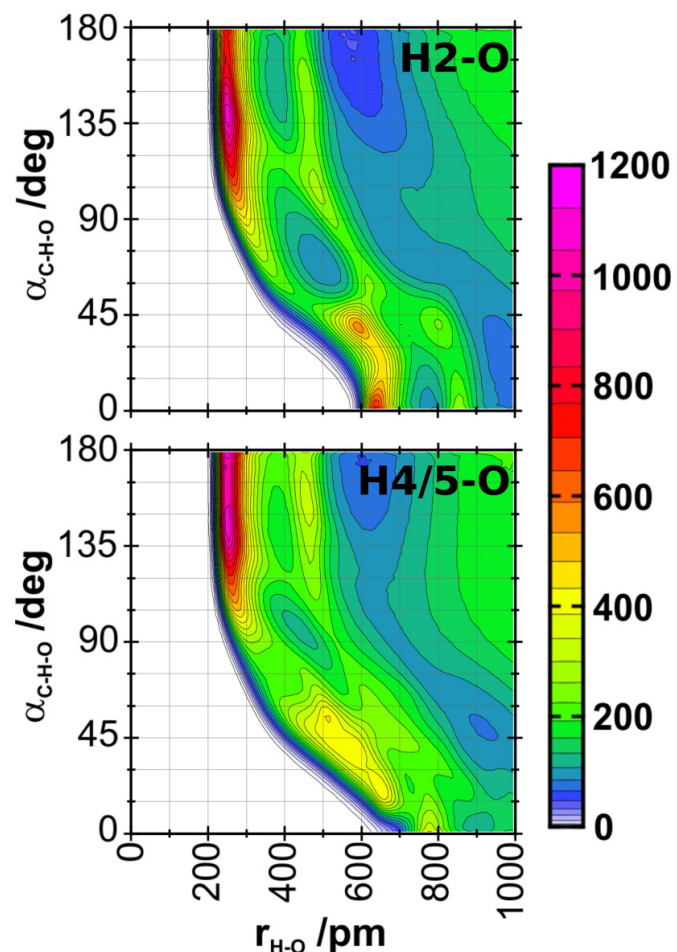


Figure 18: CDFs for occurring HB geometries in $[C_4C_1Im][OTf]$ simulated at 353 K. Donor-hydrogen-acceptor angle vs. acceptor-hydrogen distance is shown. In the upper panel the interplay between H2 and the O atoms is illustrated, in the lower the interplay between H4, H5 and the O atoms.

$[C_4C_1Im][OTf]$ at 373 K

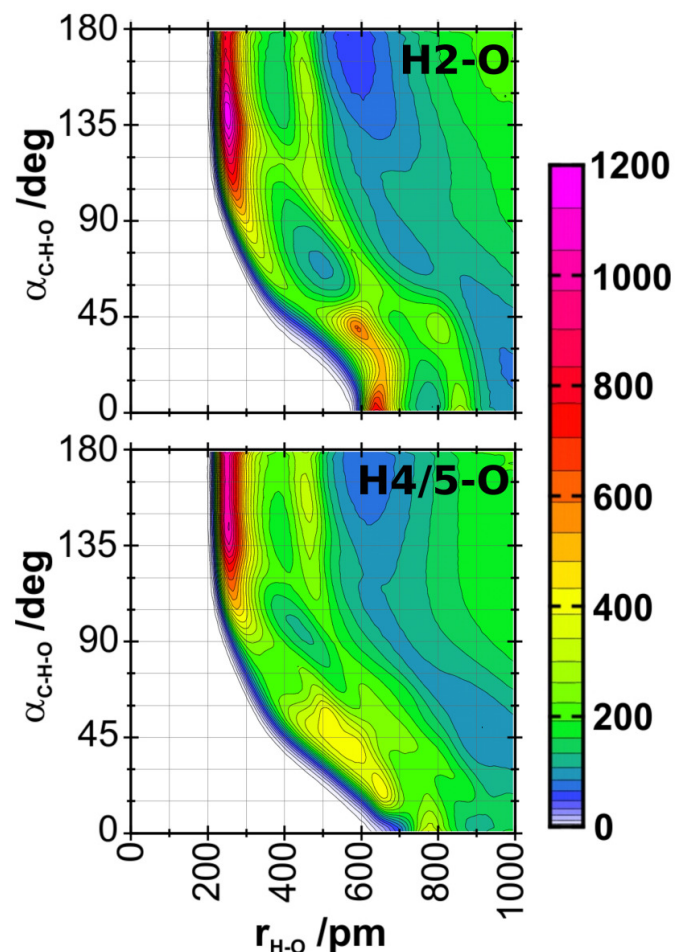


Figure 19: CDFs for occurring HB geometries in $[C_4C_1Im][OTf]$ simulated at 373 K. Donor-hydrogen-acceptor angle vs. acceptor-hydrogen distance is shown. In the upper panel the interplay between H2 and the O atoms is illustrated, in the lower the interplay between H4, H5 and the O atoms.

$[C_4C_1Im][OTf]$ at 393 K

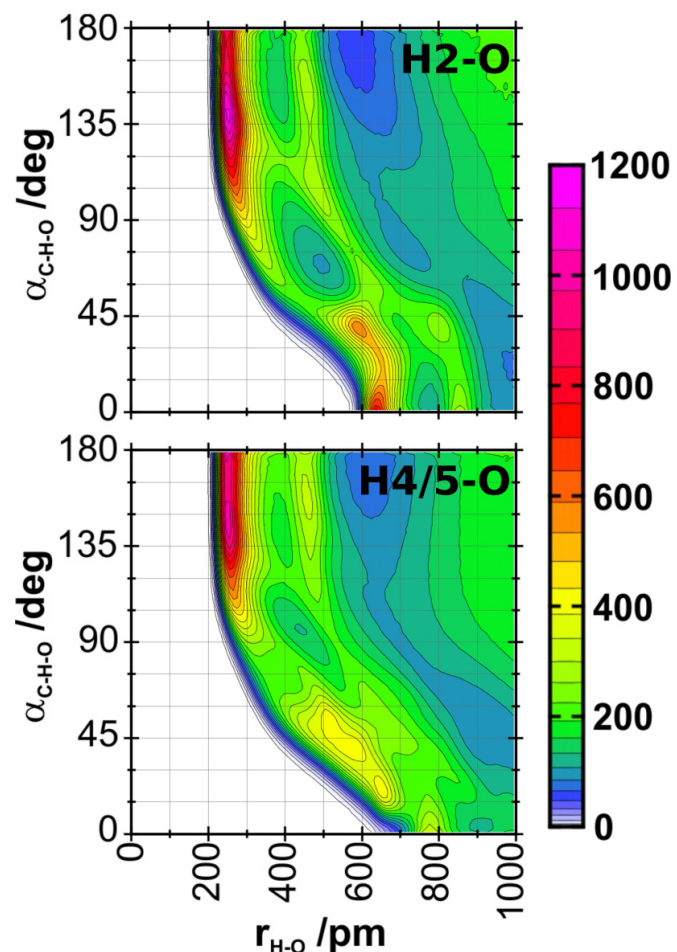


Figure 20: CDFs for occurring HB geometries in $[C_4C_1Im][OTf]$ simulated at 393 K. Donor-hydrogen-acceptor angle vs. acceptor-hydrogen distance is shown. In the upper panel the interplay between H2 and the O atoms is illustrated, in the lower the interplay between H4, H5 and the O atoms.

2.2.3 Mixture of IL with Water

IL/water $x = 0.39$ — H(w)-O

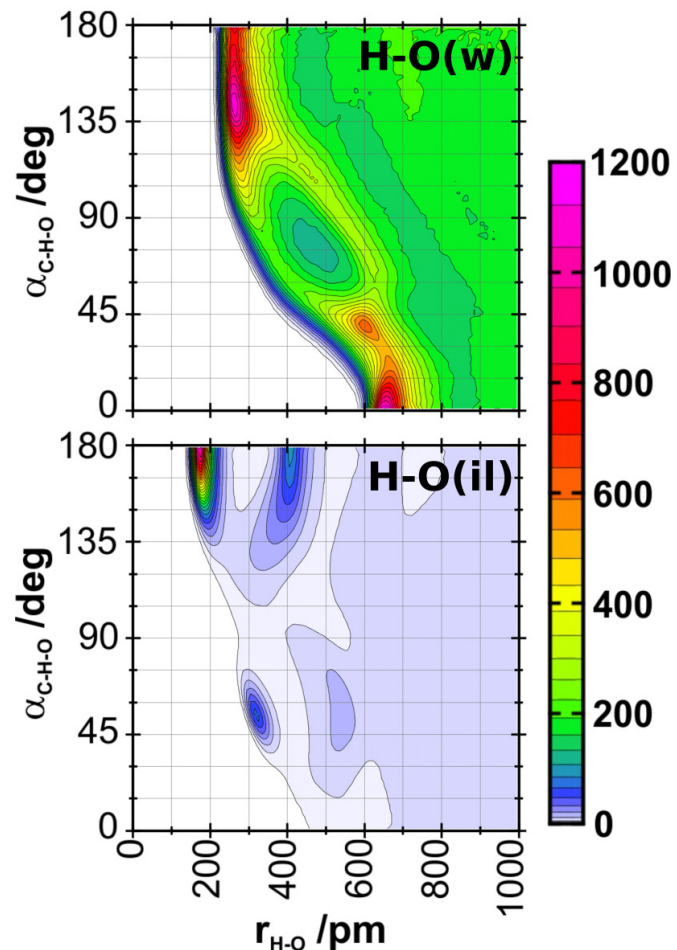


Figure 21: CDFs for occurring HB geometries in the IL/water-mixture with a mole fraction of 0.39 for the IL. Donor-hydrogen-acceptor angle vs. acceptor-hydrogen distance is shown. In the upper panel the interplay between the H atoms of the water and the O atoms of the water is illustrated, in the lower the interplay between the H atoms of the water and the O atoms of the anion.

IL/water $x = 0.39$ — H-OTf

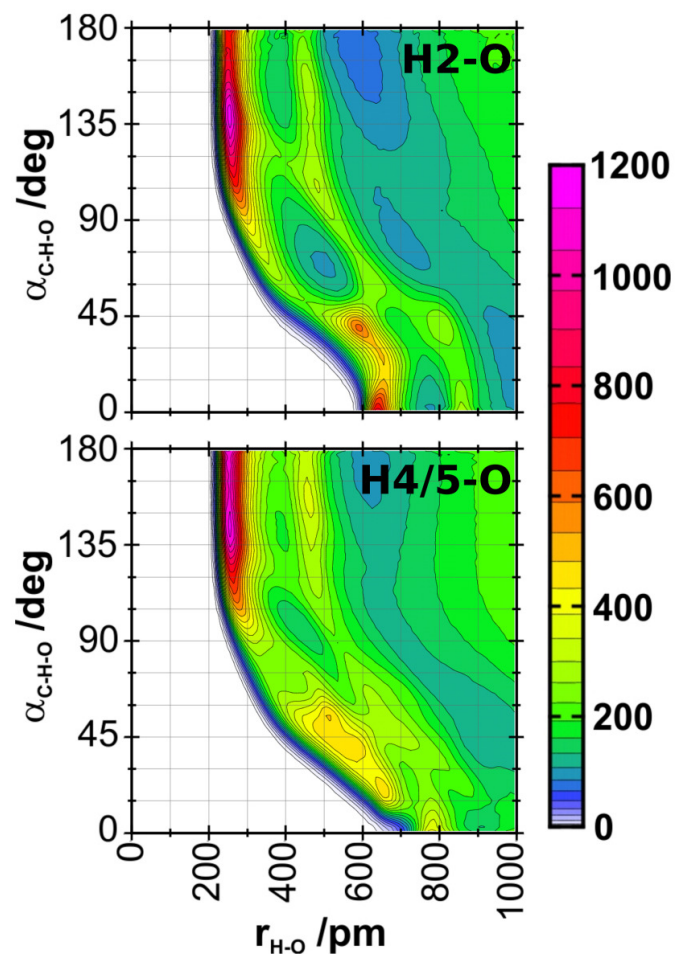


Figure 22: CDFs for occurring HB geometries in the IL/water-mixture with a mole fraction of 0.39 for the IL. Donor-hydrogen-acceptor angle vs. acceptor-hydrogen distance is shown. In the upper panel the interplay between H2 and the O atoms of the anion is illustrated, in the lower the interplay between H4, H5 and the O atoms of the anion.

IL/water $x = 0.39$ — H-O(w)

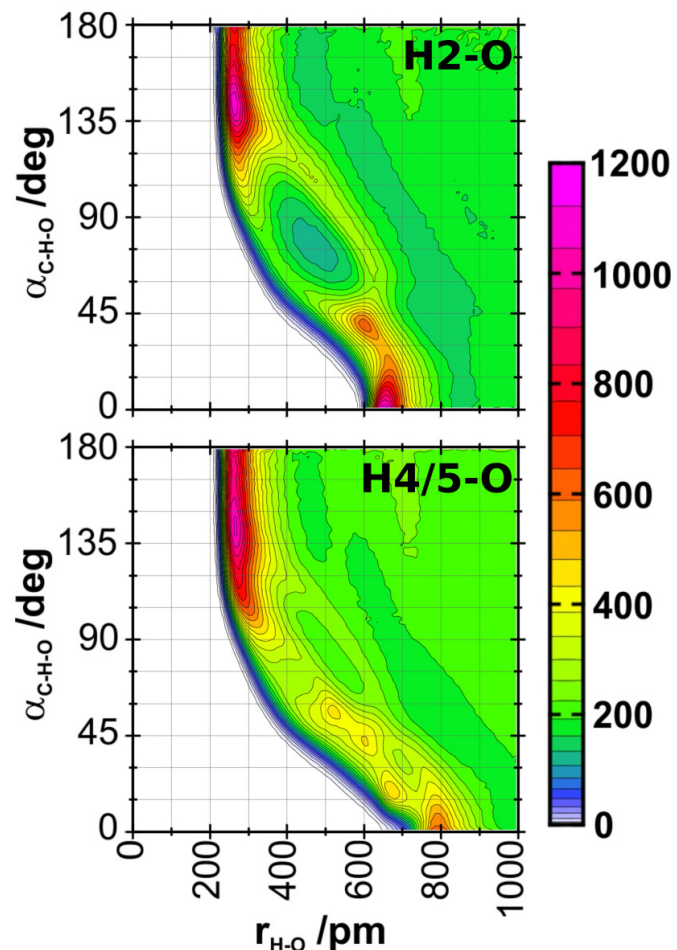


Figure 23: CDFs for occurring HB geometries in the IL/water-mixture with a mole fraction of 0.39 for the IL. Donor-hydrogen-acceptor angle vs. acceptor-hydrogen distance is shown. In the upper panel the interplay between H2 and the O atom of water is illustrated, in the lower the interplay between H4, H5 and the O atom of water.

IL/water $x = 0.58$ — H(w)-O

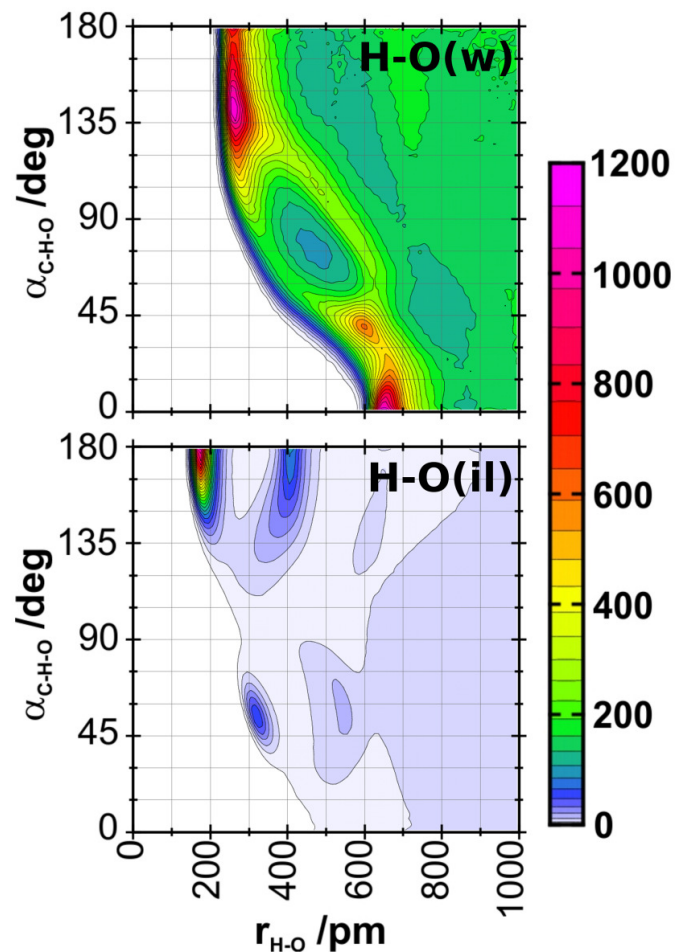


Figure 24: CDFs for occurring HB geometries in the IL/water-mixture with a mole fraction of 0.58 for the IL. Donor-hydrogen-acceptor angle vs. acceptor-hydrogen distance is shown. In the upper panel the interplay between the H atoms of the water and the O atoms of the water is illustrated, in the lower the interplay between the H atoms of the water and the O atoms of the anion.

IL/water $x = 0.58$ — H-OTf

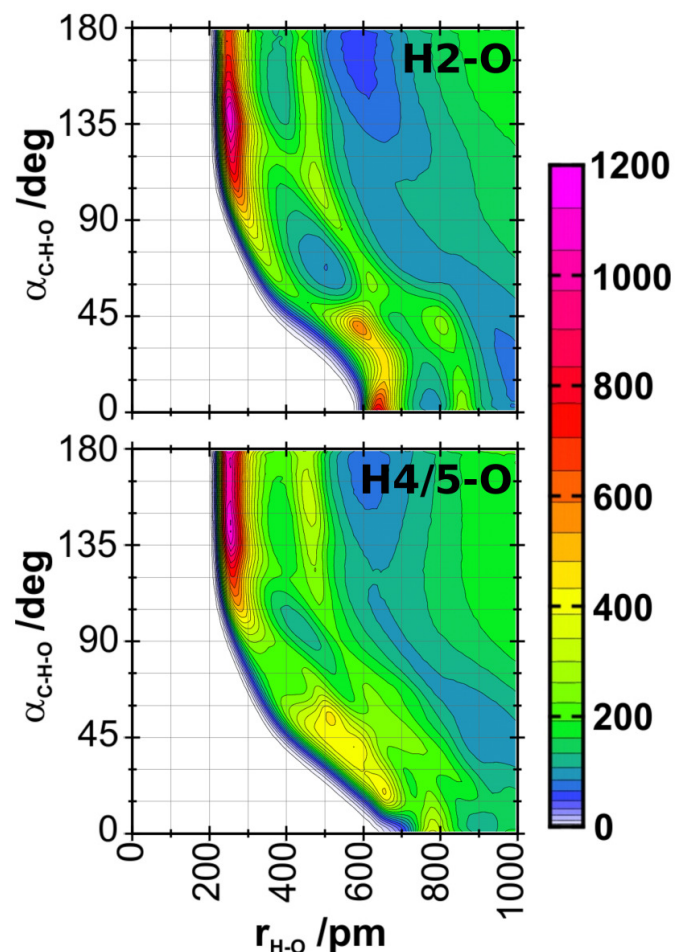


Figure 25: CDFs for occurring HB geometries in the IL/water-mixture with a mole fraction of 0.58 for the IL. Donor-hydrogen-acceptor angle vs. acceptor-hydrogen distance is shown. In the upper panel the interplay between H2 and the O atoms of the anion is illustrated, in the lower the interplay between H4, H5 and the O atoms of the anion.

IL/water $x = 0.58$ — H-O(w)

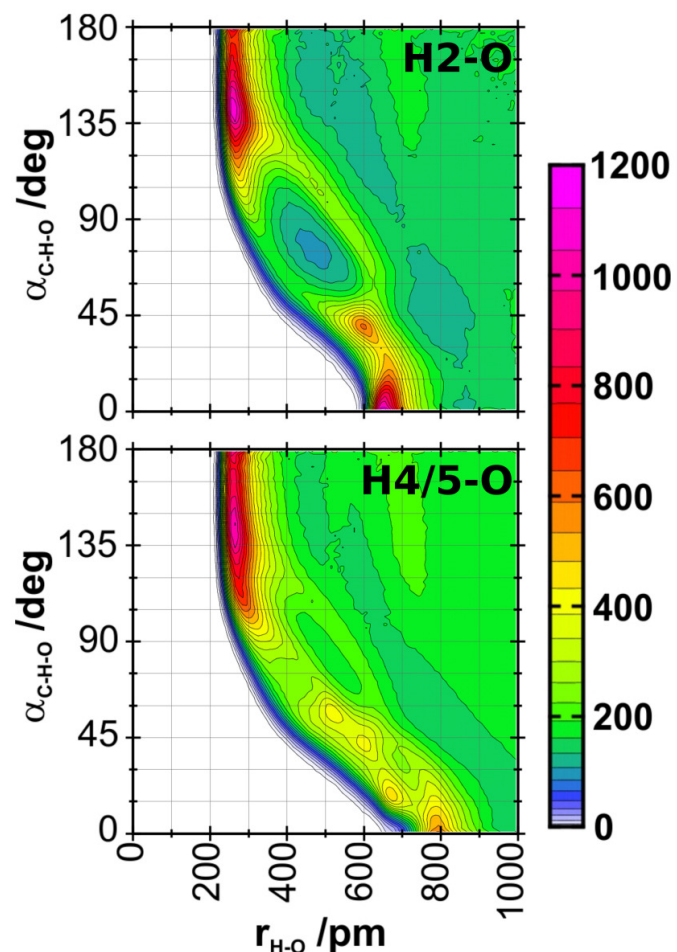


Figure 26: CDFs for occurring HB geometries in the IL/water-mixture with a mole fraction of 0.58 for the IL. Donor-hydrogen-acceptor angle vs. acceptor-hydrogen distance is shown. In the upper panel the interplay between H2 and the O atom of water is illustrated, in the lower the interplay between H4, H5 and the O atom of water.

IL/water $x = 0.66$ — H(w)-O

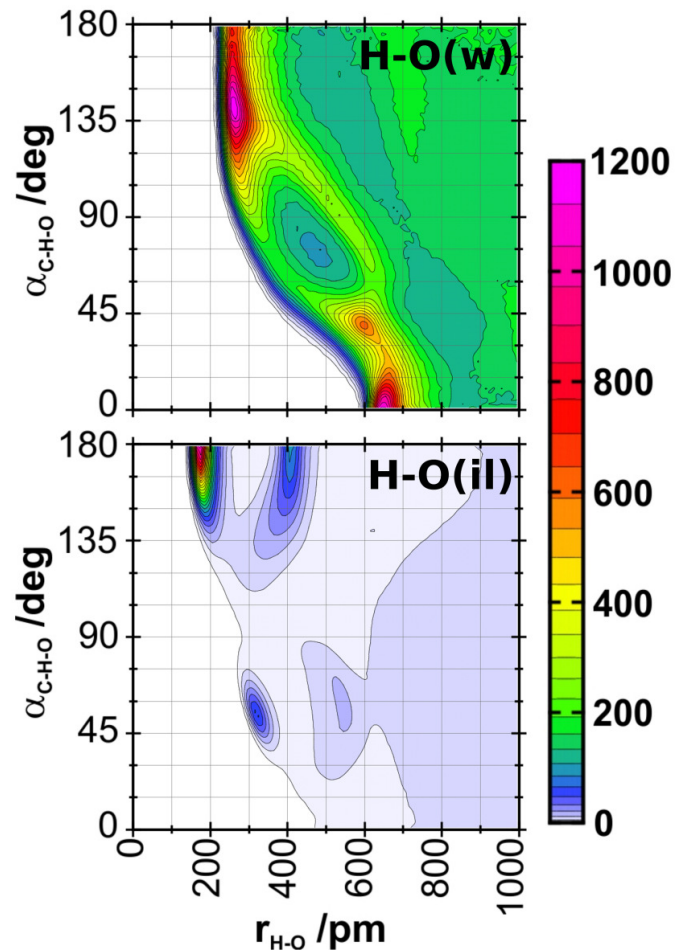


Figure 27: CDFs for occurring HB geometries in the IL/water-mixture with a mole fraction of 0.66 for the IL. Donor-hydrogen-acceptor angle vs. acceptor-hydrogen distance is shown. In the upper panel the interplay between the H atoms of the water and the O atoms of the water is illustrated, in the lower the interplay between the H atoms of the water and the O atoms of the anion.

IL/water $x = 0.66$ — H-OTf

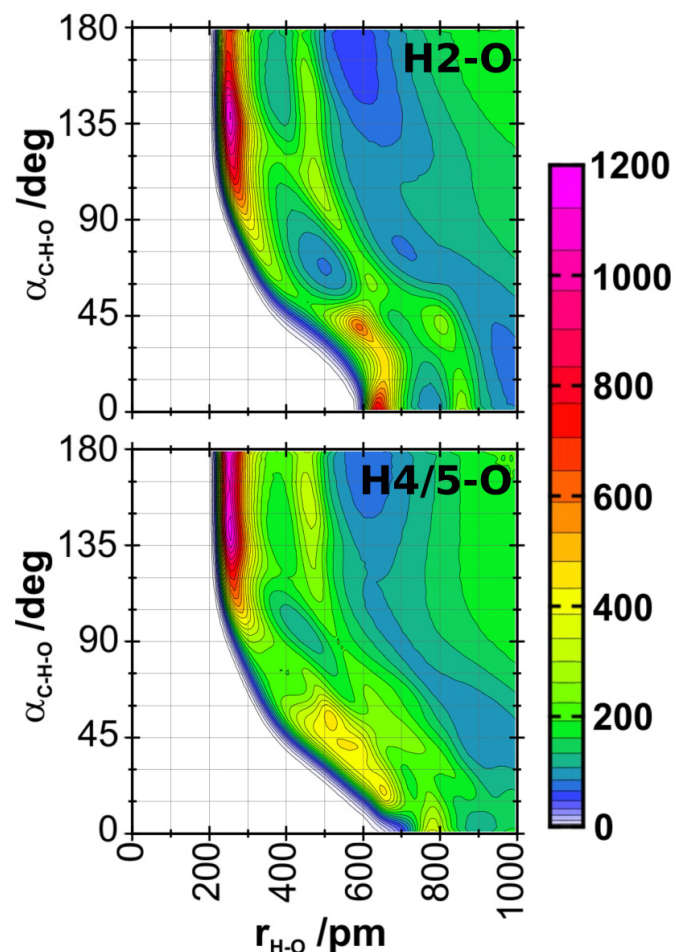


Figure 28: CDFs for occurring HB geometries in the IL/water-mixture with a mole fraction of 0.66 for the IL. Donor-hydrogen-acceptor angle vs. acceptor-hydrogen distance is shown. In the upper panel the interplay between H2 and the O atoms of the anion is illustrated, in the lower the interplay between H4, H5 and the O atoms of the anion.

IL/water $x = 0.66$ — H-O(w)

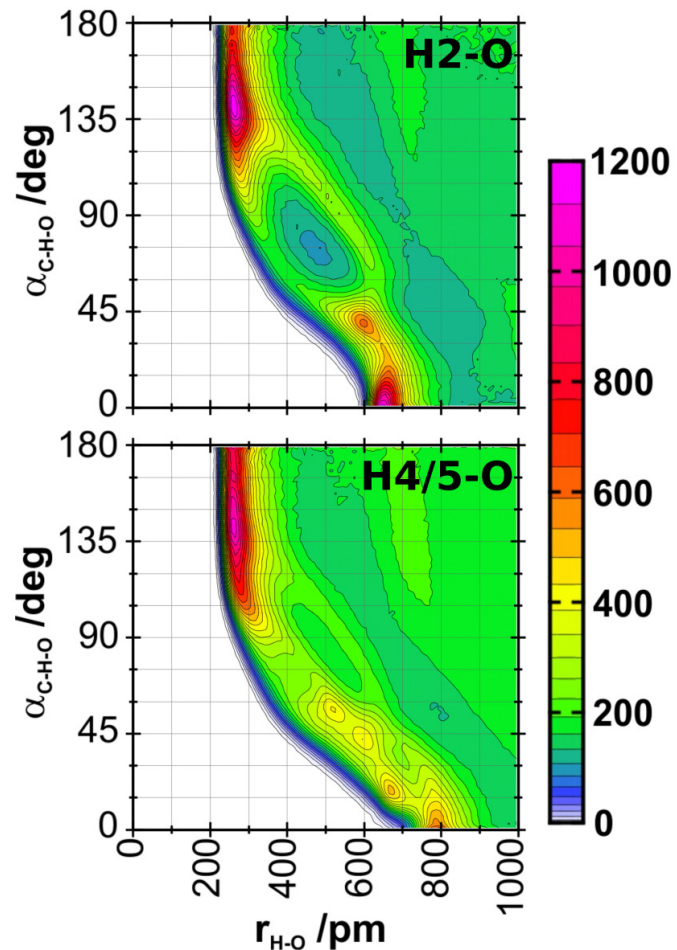


Figure 29: CDFs for occurring HB geometries in the IL/water-mixture with a mole fraction of 0.66 for the IL. Donor-hydrogen-acceptor angle vs. acceptor-hydrogen distance is shown. In the upper panel the interplay between H2 and the O atom of water is illustrated, in the lower the interplay between H4, H5 and the O atom of water.

IL/water $x = 0.82$ — H(w)-O

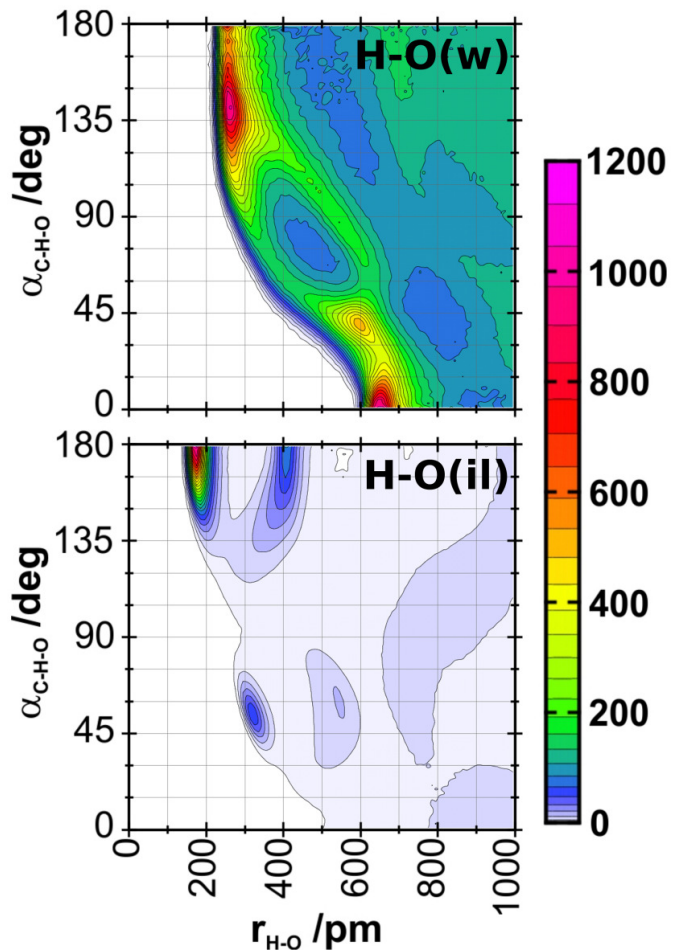


Figure 30: CDFs for occurring HB geometries in the IL/water-mixture with a mole fraction of 0.82 for the IL. Donor-hydrogen-acceptor angle vs. acceptor-hydrogen distance is shown. In the upper panel the interplay between the H atoms of the water and the O atoms of the water is illustrated, in the lower the interplay between the H atoms of the water and the O atoms of the anion.

IL/water $x = 0.82$ — H-OTf

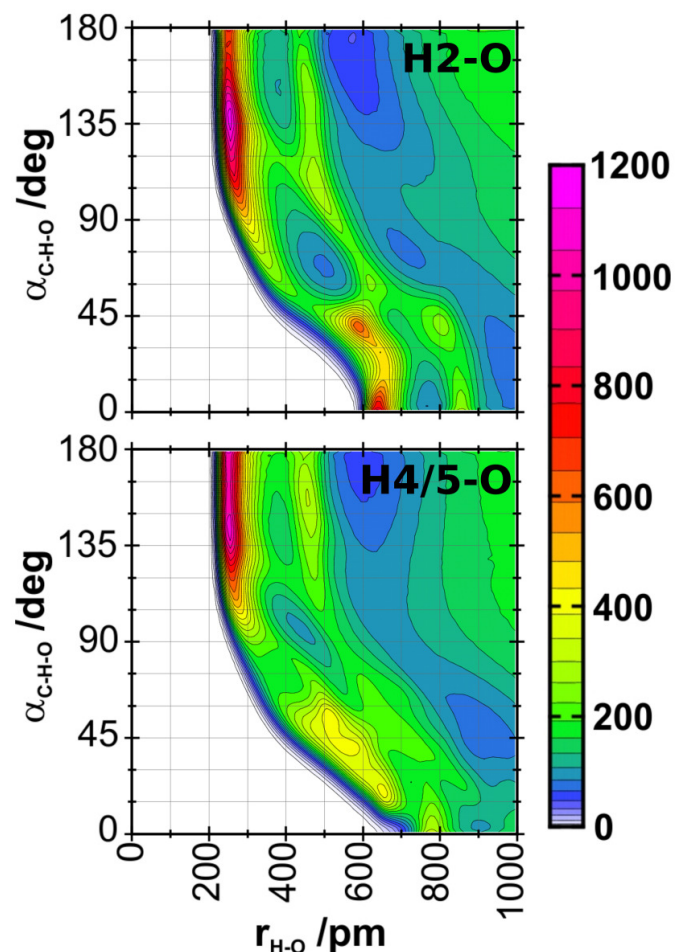


Figure 31: CDFs for occurring HB geometries in the IL/water-mixture with a mole fraction of 0.82 for the IL. Donor-hydrogen-acceptor angle vs. acceptor-hydrogen distance is shown. In the upper panel the interplay between H2 and the O atoms of the anion is illustrated, in the lower the interplay between H4, H5 and the O atoms of the anion.

IL/water $x = 0.82$ — H-O(w)

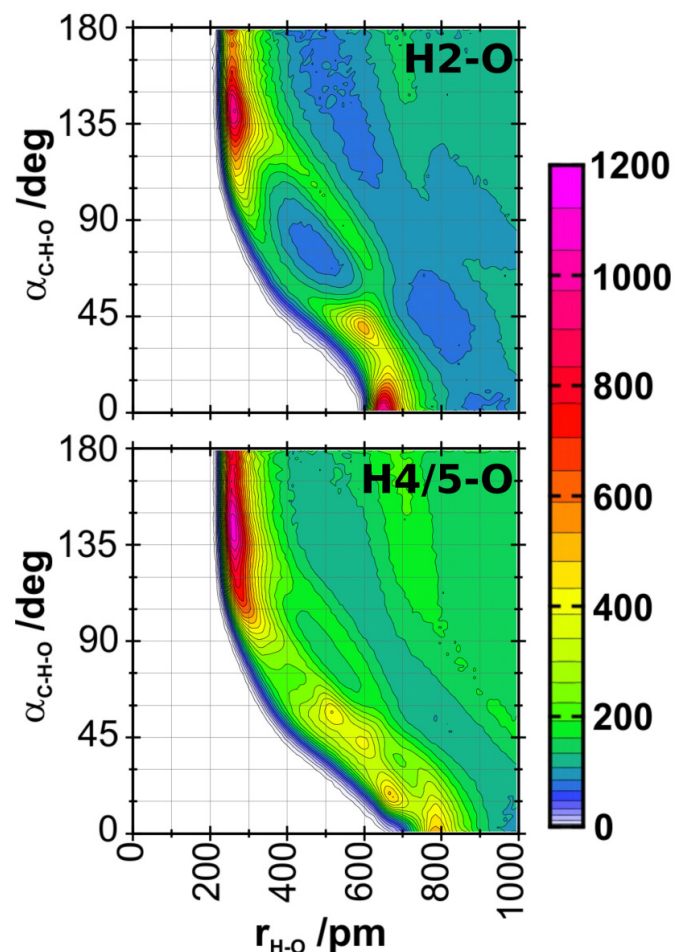


Figure 32: CDFs for occurring HB geometries in the IL/water-mixture with a mole fraction of 0.82 for the IL. Donor-hydrogen-acceptor angle vs. acceptor-hydrogen distance is shown. In the upper panel the interplay between H2 and the O atom of water is illustrated, in the lower the interplay between H4, H5 and the O atom of water.

2.2.4 Ionic Liquid Mixtures

$[C_4C_1Im][OTf]/[Cl]$ $x_{Cl} = 0.192$

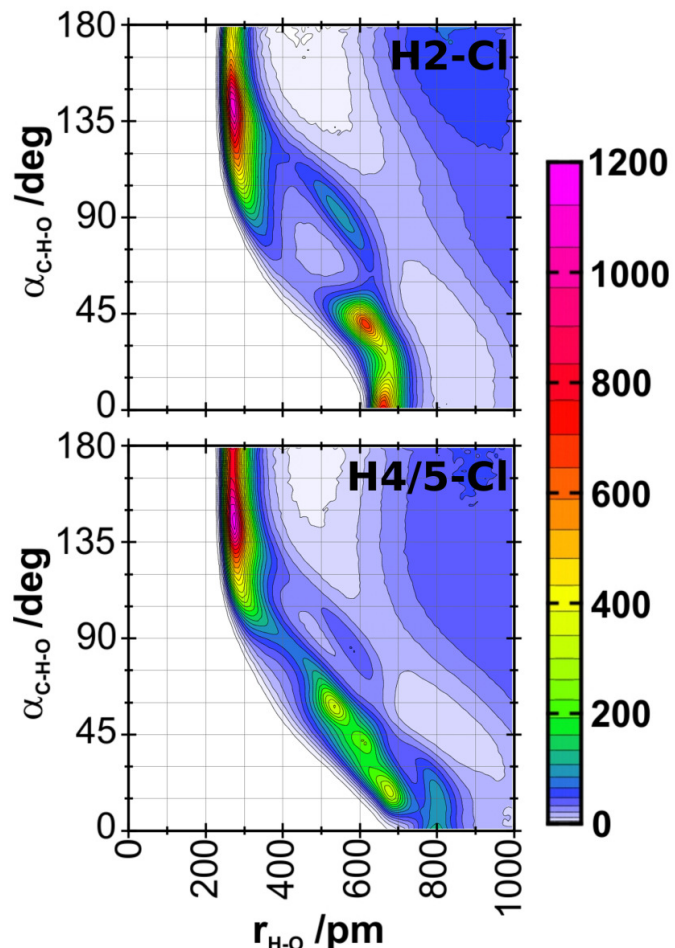


Figure 33: CDFs for occurring HB geometries in the $[C_4C_1Im][OTf]/[Cl]$ -mixture with a mole fraction of 0.192 for the chloride. Donor-hydrogen-acceptor angle vs. acceptor-hydrogen distance is shown. In the upper panel the interplay between H2 and the Cl is illustrated, in the lower the interplay between H4, H5 and the Cl.

$[C_4C_1Im][OTf]/[Cl]$ $x_{Cl} = 0.192$

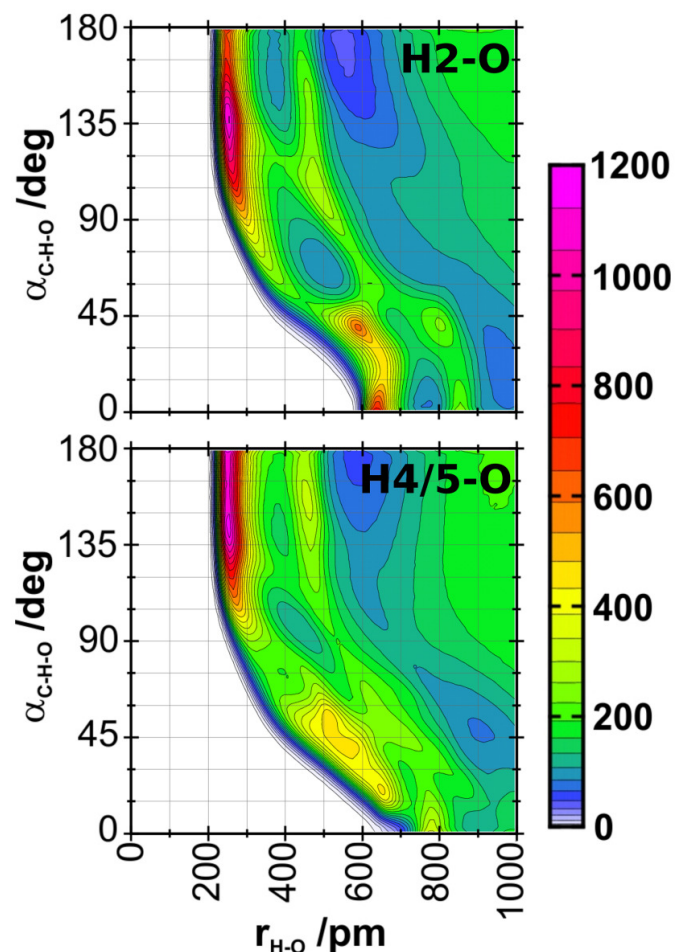


Figure 34: CDFs for occurring HB geometries in the $[C_4C_1Im][OTf]/[Cl]$ -mixture with a mole fraction of 0.192 for the chloride. Donor-hydrogen-acceptor angle vs. acceptor-hydrogen distance is shown. In the upper panel the interplay between H2 and the OTf is illustrated, in the lower the interplay between H4, H5 and the OTf.

$[C_4C_1Im][OTf]/[Cl]$ $x_{Cl} = 0.303$

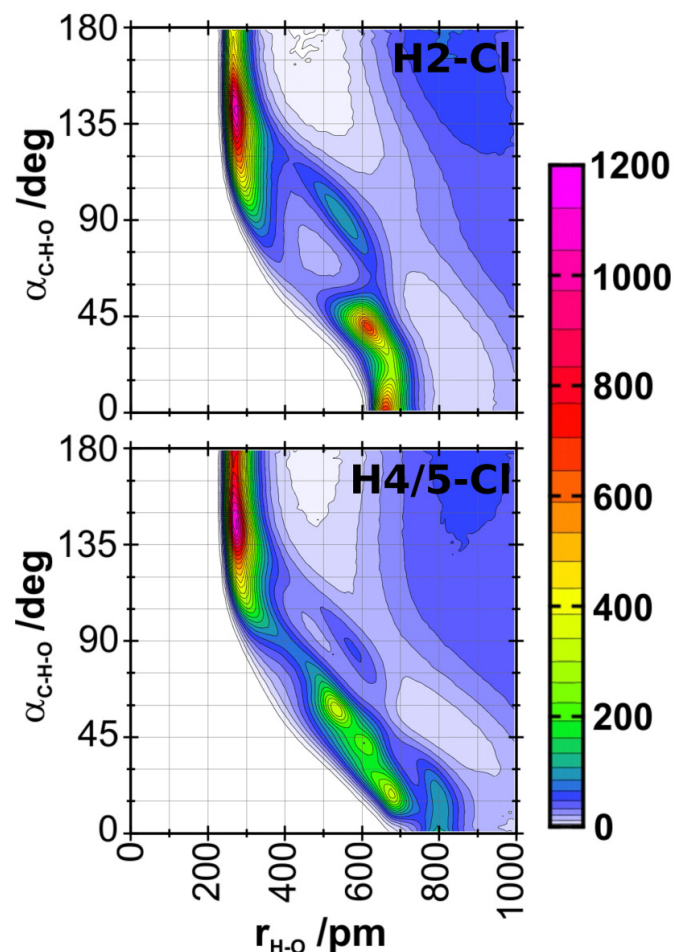


Figure 35: CDFs for occurring HB geometries in the $[C_4C_1Im][OTf]/[Cl]$ -mixture with a mole fraction of 0.303 for the chloride. Donor-hydrogen-acceptor angle vs. acceptor-hydrogen distance is shown. In the upper panel the interplay between H2 and the Cl is illustrated, in the lower the interplay between H4, H5 and the Cl.

$[C_4C_1Im][OTf]/[Cl]$ $x_{Cl} = 0.303$

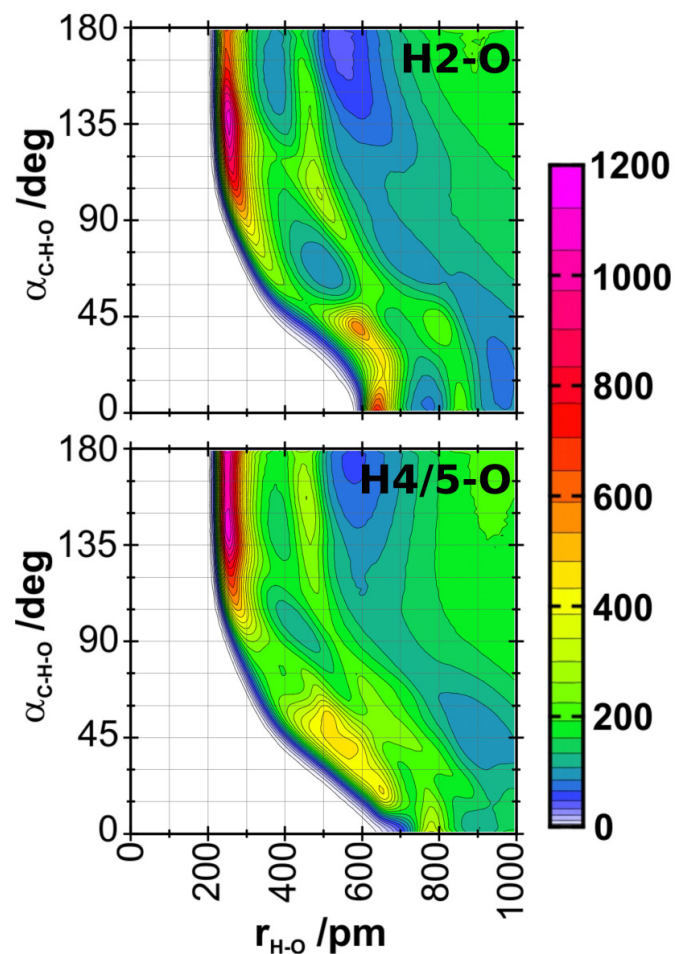


Figure 36: CDFs for occurring HB geometries in the $[C_4C_1Im][OTf]/[Cl]$ -mixture with a mole fraction of 0.303 for the chloride. Donor-hydrogen-acceptor angle vs. acceptor-hydrogen distance is shown. In the upper panel the interplay between H2 and the OTf is illustrated, in the lower the interplay between H4, H5 and the OTf.

$[C_4C_1Im][OTf]/[Cl]$ $x_{Cl} = 0.402$

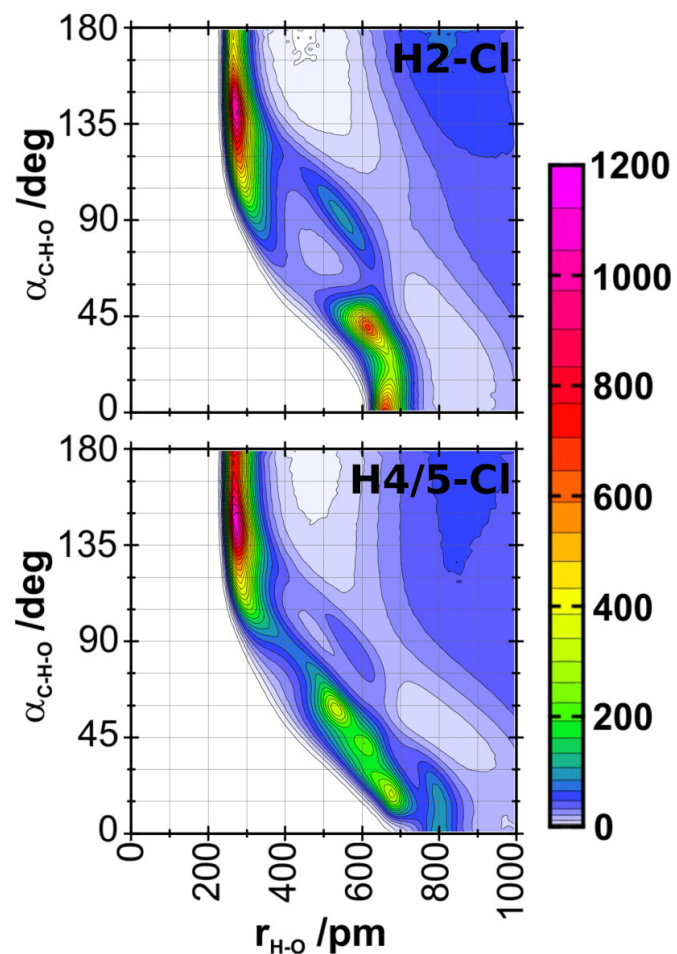


Figure 37: CDFs for occurring HB geometries in the $[C_4C_1Im][OTf]/[Cl]$ -mixture with a mole fraction of 0.402 for the chloride. Donor-hydrogen-acceptor angle vs. acceptor-hydrogen distance is shown. In the upper panel the interplay between H2 and the Cl is illustrated, in the lower the interplay between H4, H5 and the Cl.

$[C_4C_1Im][OTf]/[Cl]$ $x_{Cl} = 0.402$

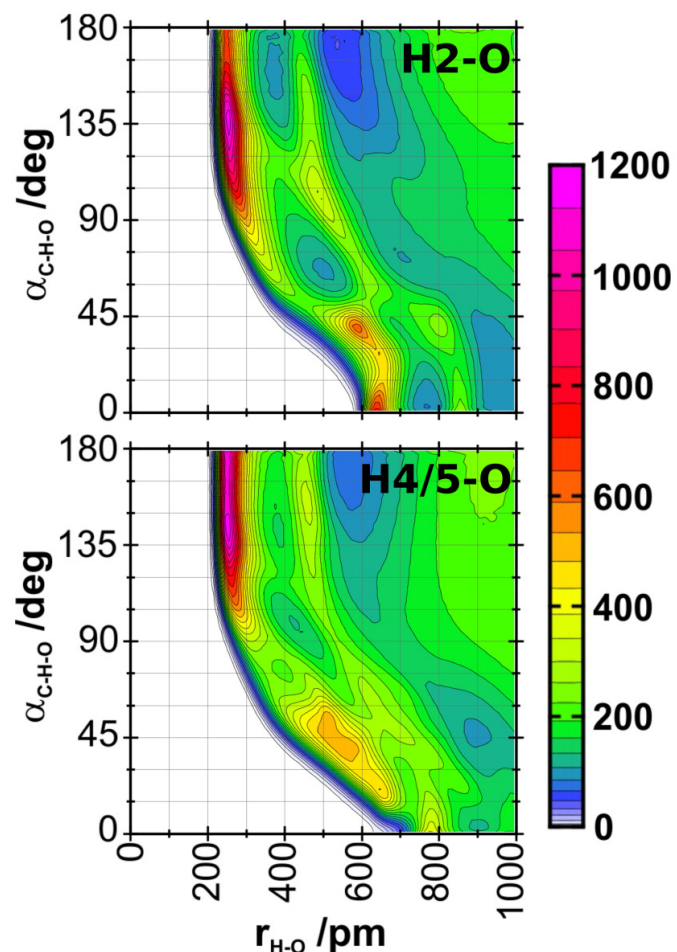


Figure 38: CDFs for occurring HB geometries in the $[C_4C_1Im][OTf]/[Cl]$ -mixture with a mole fraction of 0.402 for the chloride. Donor-hydrogen-acceptor angle vs. acceptor-hydrogen distance is shown. In the upper panel the interplay between H2 and the OTf is illustrated, in the lower the interplay between H4, H5 and the OTf.

3 Results: Dynamics

3.1 Reactive Flux Functions

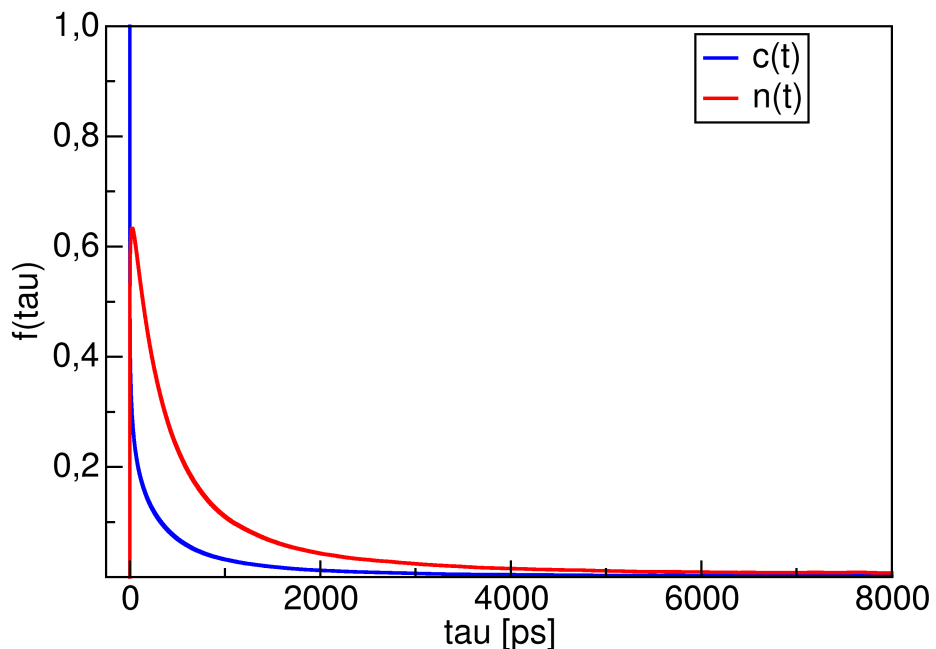


Figure 39: Correlation functions $c(t)$ and $n(t)$ of the reactive flux analysis of the pure $[C_4C_1Im][Br]$ system. In the analysis the long trajectory was selected.

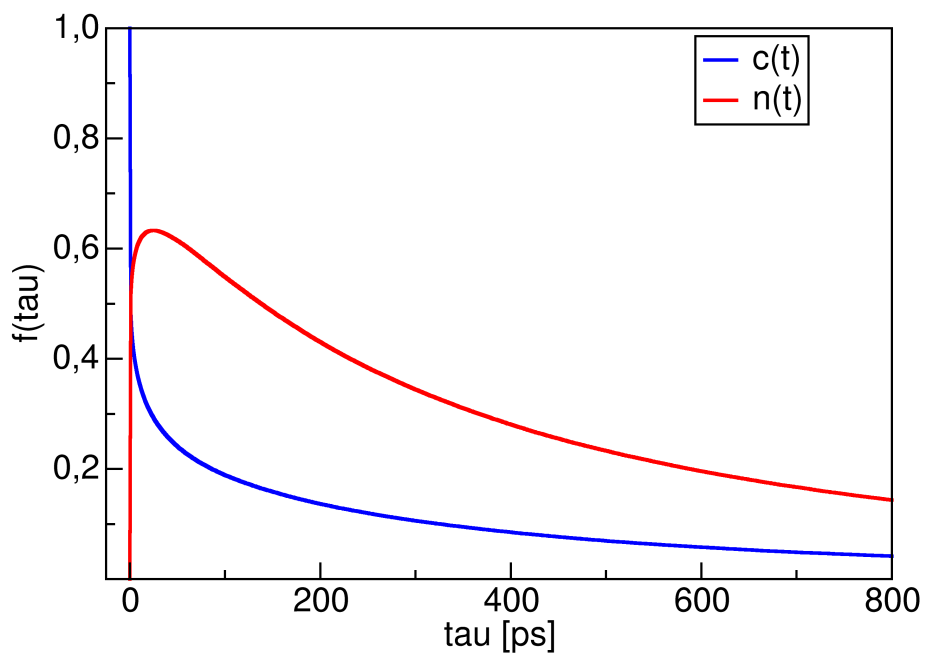


Figure 40: The first 800 ps of the correlation functions $c(t)$ and $n(t)$.

3.2 Mixtures of IL and Water

Table 4: Lifetimes of ion pair and ion cage interplay in $[C_4C_1Im][OTf]$ water mixtures.
 x_{IL} gives the mole fraction of the IL.

x_{IL}	$\tau^{c(R)-c(A)}$ (IC/IP)	continuous		
		$\tau^{c(R)-c(W)}$	$\tau^{c(W)-c(A)}$	$\tau^{c(W)-c(W)}$
0.39	153.12 / 4.58	8.15	24.39	20.81
0.58	151.48 / 3.78	16.93	18.36	42.50
0.66	157.26 / 4.07	27.27	16.80	60.46
0.82	163.07 / 3.98	61.55	15.18	80.82
x_{IL}	$\tau^{c(R)-c(A)}$ (IC/IP)	intermittent		
		$\tau^{c(R)-c(W)}$	$\tau^{c(W)-c(A)}$	$\tau^{c(W)-c(W)}$
0.39	8713.04 / 2048.13	697.79	1153.41	728.47
0.58	8873.48 / 2036.67	1243.06	1328.13	1469.96
0.66	(12105.4) / 2552.36	1620.99	1422.41	2146.28
0.82	(11852.2) / 2696.76	2736.88	1406.12	2967.58

Table 5: Hydrogen bond dynamics in $[C_4C_1Im][OTf]$ water mixtures. X gives the mole fraction of the IL.

x _{IL}	continuous		
	$\tau^{H2-O(A)}$	$\tau^{H2-O(W)}$	$\tau^{H4/5-O(A)}$
0.39	0.77	1.04	1.22
0.58	0.79	1.06	1.21
0.66	0.80	0.97	1.16
0.82	0.80	1.05	1.27
x _{IL}	$\tau^{H4/5-O(W)}$	$\tau^{H(W)-O(A)}$	$\tau^{H(W)-O(W)}$
	1.07	0.35	0.52
0.39	1.02	0.38	0.59
0.58	1.01	0.39	0.58
0.66	1.07	0.45	0.66
x _{IL}	intermittent		
	$\tau^{H2-O(A)}$	$\tau^{H2-O(W)}$	$\tau^{H4/5-O(A)}$
0.39	600.94	431.90	587.44
0.58	669.93	534.07	694.93
0.66	823.73	578.10	806.61
0.82	873.70	643.71	857.43
x _{IL}	$\tau^{H4/5-O(W)}$	$\tau^{H(W)-O(A)}$	$\tau^{H(W)-O(W)}$
	358.91	396.38	677.44
0.39	420.75	502.42	1154.99
0.58	460.36	561.70	1560.69
0.66	449.12	663.46	1620.56

3.3 Ionic Liquid Mixtures

Table 6: Lifetimes in $[C_4C_1Im][Cl]/[OTf]$ at 298 K. x = mole fraction of $[C_4C_1Im][Cl]$.

x	continuous			
	τ^{H2-O}	τ^{H2-Cl}	$\tau^{H4/5-O}$	$\tau^{H4/5-Cl}$
0.000	0.8	—	1.1	—
0.192	0.8	1.1	1.1	2.2
0.303	0.8	1.2	1.2	2.2
0.402	0.8	1.2	1.2	2.2
x	intermittent			
	τ^{H2-O}	τ^{H2-Cl}	$\tau^{H4/5-O}$	$\tau^{H4/5-Cl}$
0.000	831	—	709	—
0.192	704	2476	633	2164
0.303	1124	2901	988	3725
0.402	1316	4363	1067	3893

Table 7: Lifetimes in $[C_4C_1Im][Cl]/[OTf]$. Please note in τ^{IP} and τ^{IC} we do not distinguish the anion type. x gives the mole fraction of $[C_4C_1Im][Cl]$. The first block gives the ion cage dynamics results with different function types and obtained from different trajectories. The second block gives the intermittent results obtained from the short 200 ps trajectory.

Cage dynamics			
x	$\tau_{\text{continuous}}^{\text{IC}}$	$\tau_{\text{200ps}}^{\text{IC}}$	$\tau_{\text{10ns}}^{\text{IC}}$
0.000	169.87	(9192.7)	(10639.4)
0.192	141.98	(6484.2)	8789.3
0.303	156.68	(4743.2)	(23701.4)
0.402	166.22	(5891.8)	(19625.2)

intermittent with 200 ps					
x	$\tau^{\text{H}_2-\text{O}}$	$\tau^{\text{H}_2-\text{Cl}}$	$\tau^{\text{H}_4/\text{5}-\text{O}}$	$\tau^{\text{H}_4/\text{5}-\text{Cl}}$	τ^{IP}
0.000	(296.00)	—	(236.87)	—	(607.60)
0.192	156.13	(553.60)	179.79	(716.02)	(553.88)
0.303	168.17	(649.91)	(219.55)	(633.90)	(449.38)
0.402	(221.25)	(950.22)	(255.60)	(1379.84)	(637.22)

4 Results: Correlating Viscosity with Ion Pair Dynamics

4.1 Experimental and Calculated Viscosities

Table 8: Experimental and calculated viscosities for $[C_4C_1Im][OTf]$ at different mole temperatures. First column: temperature; Second: ion pair dynamics; Third: group contribution method GC²⁵; 4th: experimental data; Last: simulated data. First block: temperature dependent data. Second block: $[C_4C_1Im][OTf]$ /water mixture. x gives the molefraction of the IL. Third block: IL mixtures. x gives the mole fraction of $[C_4C_1Im][Cl]$

in K T	in ps τ_I^{IP}	GC	Exp	η in Pa·s	calc
298.15	0.0655		$0.0832 \pm 0.0025^{26} / 0.0928 \pm 0.0043^{27}$ $0.0907 \pm 0.0038^{27} / 0.088 \pm 0.011^{28}$ (298.15-328.15 K) 0.0866 ± 0.0027^{29} (298.15-343.15 K) 0.0844 ± 0.0085^{30} (298.15-353.15 K)		
293	0.0823		$0.112 \pm 0.011^{30} / 0.138 \pm 0.039^{17}$ (283.1-363.15 K)	0.00241	
323	0.0260		$0.0308 \pm 0.0031^{30} / 0.0281 \pm 0.002^{17}$ $0.0316 \pm 0.001^{29} / 0.0296 \pm 0.002^{18}$ (303.15 to 343.15 K)	0.00200	
353	0.0118		$0.013 \pm 0.0013^{30} / 0.01192 \pm 0.00088^{17}$	0.00166	
373	0.0079			0.00144	
393	0.0057			0.00134	
x	in ps τ_I^{IP}	GC	Exp	η in Pa·s	calc
0.39	—		0.0155 (0.4077, 303 K) ¹⁸	0.00232	
0.58	—		0.0232 (0.6001, 303 K) ¹⁸	0.00246	
0.66	—		0.0290 (0.7013, 303 K) ¹⁸	0.00232	
0.82	—		0.0354 (0.8061, 303 K) ¹⁸	0.00243	
x	in ps τ_I^{IP}	GC	Exp	η in Pa·s	calc
0.000	—		0.05816 (298.15 K) ¹⁹	0.00219	
0.192	—		0.07887 (298.15 K) ¹⁹	0.00202	
0.303	—		0.10410 (298.15 K) ¹⁹	0.00250	
0.402	—		0.20367 (298.15 K) ¹⁹	0.00259	

5 Experimental Setup

5.1 Mixture Synthesis

All reagents and solvents were bought from Sigma Aldrich and used as described without further purification. To make $[C_4C_1Im][OTf]$, freshly distilled methyltrifluoromethanesulfonate (15.81 g, 96.34 mmol, 1.02 eq.) was added drop wise to a solution of 1-butylimidazole (11.73 g, 94.45 mmol, 1 eq.) in acetonitrile (20 mL) at 0°C under vigorous stirring. The reaction mixture was allowed to come to room temperature over 4 hours, still under vigorous stirring. Then the excess reagents and solvents were removed in vacuo to give a clear colourless liquid (27.09 g, 99% yield).

To make $[C_4C_1Im]Cl$, 1-chlorobutane (19.08 g, 206 mmol, 1.2 eq.) was added drop wise to a solution of 1-methyimidazole (14.10 g, 172 mmol, 1 eq.) in acetonitrile (20 mL). The reaction mixture was heated to 60°C under gentle stirring for 115 hours, after which the mixture was cooled to –20°C for 24 hours. The product was precipitated by addition of ethyl acetate and was recrystallized with acetonitrile and ethyl acetate (approximately 1:15) five times, affording a white solid. This solid was then dried in vacuo at 50°C for 24 hours to give a white powder (17.35 g, 58% yield).

To make the mixtures, $[C_4C_1Im]Cl$ was placed in a sample vial, then dried overnight at 50°C and weighed to find the exact amount of dry $[C_4C_1Im]Cl$ used. Then, the appropriate amount of $[C_4C_1Im][OTf]$ was added to create the mixtures with the compositions listed in table 1. The mixtures were mixed at 50°C until homogeneous, then dried in vacuo at 50°C overnight. Karl-Fischer measurements of water content were performed using a Mettler Toledo C20 Coulometer, and the results are shown in Tab. 9.

Note that all 1D proton NMR spectra were checked for water and no measurable water was found to be present in these samples.

Table 9: Mixture details of the two sets of mixtures used.

Mixture	Ratio of $[C_4C_1Im][OTf]:[C_4C_1Im]Cl$	Water Content
A	1.000:0.000 1.000:0.000	273 ppm 86.7 ppm
B	0.810:0.190 0.809:0.191	127 ppm 58.6 ppm
C	0.692:0.308 0.697:0.303	153 ppm 115 ppm
D	0.600:0.400 0.598:0.402	709 ppm 102 ppm

5.2 NMR Measurements

All samples were measured on a Bruker Avance III NMR spectrometer at 500 MHz. Proton and fluorine 1D measurements were taken for all samples, then the PFGSTE measurements also known as DOSY, were made. ^{35}Cl measurements were attempted, however the width of the peaks found (300 Hz) meant that DOSY measurements could not be accurately be performed. All data was then plotted and fitted to the Stejskal–Tanner equation³¹

$$S = S_0 \exp \left(-\gamma^2 G^2 \delta^2 \left(\Delta - \frac{\delta}{3} \right) D \right) \quad (1)$$

with the measured signal intensity S , the intensity at zero applied field S_0 , the gyromagnetic ratio γ , the applied gradient field strength G , the length of applied field δ , the delay between field pulses Δ , and the diffusion coefficient D , which relates applied field strength to diffusion.

From a plot of G^2 vs $\ln(S)$ a linear relationship can be found, and the diffusion coefficient calculated. Unless specified, samples were run using $\Delta = 0.1999$ s and $\delta = 0.01$ s. γ values used were 25172 rad s $^{-1}$ Gs $^{-1}$ for ^{19}F and 26752 rad s $^{-1}$ Gs $^{-1}$ for ^1H . For ^{19}F , 16 equally spaced values of G from 0.869 Gs m $^{-1}$ to 41.271 Gs m $^{-1}$ were used. For ^1H , 24 equally spaced values of G from 0.869 Gs m $^{-1}$ to 41.271 Gs m $^{-1}$ were used.

5.3 Diffusion Summary

Usually the H2 is used for the measurements of the cation's diffusion, however any hydrogen can be used. The results show uncertainties in the H2 measurements, potentially due to traces of water. For this reason, we have chosen to evaluate the signal of the hydrogen atoms at the methyl group, because they should be less sensitive to water. To obtain the diffusion data of the anion measurements on the fluorine atoms were performed.

5.3.1 Temperature dependence

Table 10: Chemical shifts and diffusion coefficients for the cation of the pure $[\text{C}_4\text{C}_1\text{Im}][\text{OTf}]$ at different temperatures.

Temperature in K	^1H Chemical Shift in ppm	Diffusion Coefficient in m^2s^{-1}	Δ in s	δ in s
293	3.365 ± 0.008	$1.35 \pm 0.02 \text{ e-11}$	0.1999	0.01
323	3.360 ± 0.003	$4.68 \pm 0.04 \text{ e-11}$	0.499	0.01
353	3.363 ± 0.001	$1.14 \pm 0.01 \text{ e-10}$	0.499	0.007
373	3.368 ± 0.001	$1.62 \pm 0.02 \text{ e-10}$	0.499	0.006
393	3.368 ± 0.001	$3.03 \pm 0.01 \text{ e-10}$	0.499	0.005

Table 11: Chemical shifts and diffusion coefficients for the anion of the pure $[C_4C_1Im][OTf]$ at different temperatures.

Temperature in K	^{19}F Chemical Shift in ppm	Diffusion Coefficient in m^2s^{-1}	Δ in s	δ in s
293	-80.030 ± 0.004	$5.45 \pm 0.17 e-12$	0.1999	0.01
323	-79.763 ± 0.002	$2.72 \pm 0.02 e-11$	0.499	0.01
353	-79.437 ± 0.001	$8.95 \pm 0.04 e-11$	0.499	0.0064
373	-79.222 ± 0.001	$1.53 \pm 0.02 e-10$	0.499	0.0058
393	-79.004 ± 0.002	$1.12 \pm 0.03 e-10$	0.499	0.0046

5.3.2 Ionic liquid mixtures

Table 12: Chemical shifts and diffusion coefficients for the cation of the $[C_4C_1Im][Cl]/[OTf]$ mixtures.

Mixture	x [Cl]	1H Chemical Shift in ppm	Diffusion Coefficient in m^2s^{-1}
A	0.000	3.365 ± 0.008	$1.35 \pm 0.02 e-11$
B	0.192	3.389 ± 0.001	$7.31 \pm 0.15 e-12$
C	0.303	3.416 ± 0.003	$4.71 \pm 0.15 e-12$
D	0.402	3.455 ± 0.002	$3.13 \pm 0.14 e-12$

Table 13: Chemical shifts and diffusion coefficients for the anion of the $[C_4C_1Im][Cl]/[OTf]$ mixtures.

Mixture	x [Cl]	^{19}F Chemical Shift in ppm	Diffusion Coefficient in m^2s^{-1}
A	0.000	-80.030 ± 0.004	$5.45 \pm 0.17 e-12$
B	0.192	-79.973 ± 0.007	$4.14 \pm 0.90 e-12$
C	0.303	-79.930 ± 0.011	$3.06 \pm 0.38 e-12$
D	0.402	-79.895 ± 0.006	$1.82 \pm 0.07 e-12$

5.4 Detailed Diffusion Results

All results are given in the form: Experiment 1|Experiment 2

5.4.1 Temperature dependence

293 K

Table 14: Chemical shifts and diffusion coefficients for the pure $[C_4C_1Im][OTf]$ at 293 K.

Atom	Chemical Shift in ppm	Diffusion Coefficient in $m^2 s^{-1}$
H2	8.3256 8.3279	1.360e-11 1.323e-11
H4	7.1027 7.1040	1.401e-11 1.350e-11
H5	7.0281 7.0305	1.394e-11 1.358e-11
H6	3.3725 3.3571	1.366e-11 1.329e-11
H7	3.6159 3.6298	1.466e-11 1.314e-11
H8	1.2455 1.2465	1.147e-11 1.301e-11
H9	0.6960 0.6970	1.376e-11 1.330e-11
H10	0.2548 0.2553	1.405e-11 1.317e-11
F	-80.0267 -80.0337	5.287e-12 5.621e-12

323 K

Table 15: Chemical shifts and diffusion coefficients for the pure $[C_4C_1Im][OTf]$ at 323 K.

Atom	Chemical Shift in ppm	Diffusion Coefficient in $m^2 s^{-1}$
H2	8.3079 8.3140	4.487e-11 4.604e-11
H4	7.0804 7.0858	4.596e-11 4.636e-11
H5	7.0079 7.0114	4.747e-11 4.760e-11
H6	3.3567 3.3635	4.649e-11 4.719e-11
H7	3.6198 3.6372	4.590e-11 4.783e-11
H8	1.2615 1.2676	4.668e-11 4.736e-11
H9	0.7198 0.7260	4.672e-11 4.711e-11
H10	0.2708 0.2771	4.829e-11 4.595e-11
F	-79.7650 -79.7602	2.737e-11 2.706e-11

353 K

Table 16: Chemical shifts and diffusion coefficients for the pure $[C_4C_1Im][OTf]$ at 353 K.

Atom	Chemical Shift in ppm	Diffusion Coefficient in m^2s^{-1}
H2	8.2927 8.2948	1.099e-10 1.084e-10
H4	7.0602 7.0619	1.180e-10 1.145e-10
H5	6.9860 6.9877	1.136e-10 1.142e-10
H6	3.3626 3.3642	1.136e-10 1.138e-10
H7	3.6386 3.6402	1.167e-10 1.061e-10
H8	1.2825 1.2839	1.215e-10 1.203e-10
H9	0.7490 0.7507	1.201e-10 1.195e-10
H10	0.2912 0.2945	1.163e-10 1.118e-10
F	-79.4372 -79.4361	8.990e-11 8.914e-11

373 K

Table 17: Chemical shifts and diffusion coefficients for the pure $[C_4C_1Im][OTf]$ at 373 K.

Atom	Chemical Shift in ppm	Diffusion Coefficient in m^2s^{-1}
H2	8.2832 8.2866	1.212e-10 1.880e-10
H4	7.0476 7.0506	1.917e-10 1.867e-10
H5	6.9743 6.9773	1.591e-10 1.623e-10
H6	3.3662 3.3690	1.634e-10 1.602e-10
H7	3.6433 3.6462	1.920e-10 1.856e-10
H8	1.2930 1.2972	2.023e-10 2.008e-10
H9	0.7652 0.7686	1.356e-10 1.418e-10
H10	0.3028 0.3053	1.448e-10 1.485e-10
F	-79.2216 -79.2215	1.547e-10 1.522e-10

393 K

Table 18: Chemical shifts and diffusion coefficients for the pure $[C_4C_1Im][OTf]$ at 393 K.

Atom	Chemical Shift in ppm	Diffusion Coefficient in $m^2 s^{-1}$
H2	8.2715 8.2724	2.360e-10 2.503e-10
H4	7.0329 7.0335	2.913e-10 2.990e-10
H5	6.9607 6.9613	2.120e-10 2.214e-10
H7	3.6454 3.6460	1.899e-10 2.015e-10
H6	3.3673 3.3679	3.021e-10 3.044e-10
H8	1.3033 1.2926	2.365e-10 2.470e-10
H9	0.7795 0.7800	2.653e-10 2.677e-10
H10	0.3111 0.3114	2.066e-10 2.085e-10
F	-79.0063 -79.0022	1.147e-10 1.089e-10

5.4.2 Ionic liquid mixtures

Mixture A

Table 19: Chemical shifts and diffusion coefficients for Mixture A.

Atom	Chemical Shift in ppm	Diffusion Coefficient in $m^2 s^{-1}$
H2	8.3256 8.3279	1.360e-11 1.323e-11
H4	7.1027 7.1040	1.401e-11 1.350e-11
H5	7.0281 7.0305	1.394e-11 1.358e-11
H6	3.3725 3.3571	1.366e-11 1.329e-11
H7	3.6159 3.6298	1.466e-11 1.314e-11
H8	1.2455 1.2465	1.147e-11 1.301e-11
H9	0.6960 0.6970	1.376e-11 1.330e-11
H10	0.2548 0.2553	1.405e-11 1.317e-11
F	-80.0267 -80.0337	5.287e-12 5.621e-12

Mixture B

Table 20: Chemical shifts and diffusion coefficients for Mixture B.

Atom	Chemical Shift in ppm	Diffusion Coefficient in m^2s^{-1}
H2	8.7440 8.7425	7.563e-12 7.096e-12
H4	7.2835 7.2843	7.557e-12 7.047e-12
H5	7.2072 7.2081	7.588e-12 7.086e-12
H6	3.3892 3.3894	7.564e-12 7.155e-12
H7	3.6754 3.6758	7.255e-12 7.600e-12
H8	1.2271 1.2279	7.509e-12 7.092e-12
H9	0.6545 0.6550	7.498e-12 7.068e-12
H10	0.2136 0.2141	7.420e-12 7.092e-12
F	-79.9655 -79.9801	5.039e-12 3.231e-12

Mixture C

Table 21: Chemical shifts and diffusion coefficients for Mixture C.

Atom	Chemical Shift in ppm	Diffusion Coefficient in m^2s^{-1}
H2	8.9874 8.9732	4.817e-12 4.551e-12
H4	7.4082 7.4000	4.819e-12 4.542e-12
H5	7.3261 7.3183	4.840e-12 4.560e-12
H6	3.4182 3.4128	4.857e-12 4.559e-12
H7	3.7114 3.7061	4.809e-12 4.586e-12
H8	1.2217 1.2182	4.806e-12 4.648e-12
H9	0.6340 0.6306	4.694e-12 4.505e-12
H10	0.1935 0.1904	4.803e-12 4.513e-12
F	-79.9186 -79.9410	2.674e-12 3.440e-12

Mixture D

Table 22: Chemical shifts and diffusion coefficients for Mixture D.

Atom	Chemical Shift in ppm	Diffusion Coefficient in m^2s^{-1}
H2	9.1527 9.1571	3.252e-12 2.998e-12
H4	7.4975 7.5029	3.226e-12 2.965e-12
H5	7.4096 7.4151	3.252e-12 3.004e-12
H6	3.4315 3.4354	3.268e-12 2.983e-12
H7	3.7288 3.7333	3.195e-12 2.750e-12
H8	1.2055 1.2100	3.223e-12 2.980e-12
H9	0.6052 0.6088	3.084e-12 2.860e-12
H10	0.1664 0.1696	3.943e-12 2.999e-12
F	-79.8893 -79.9014	1.891e-12 1.749e-12

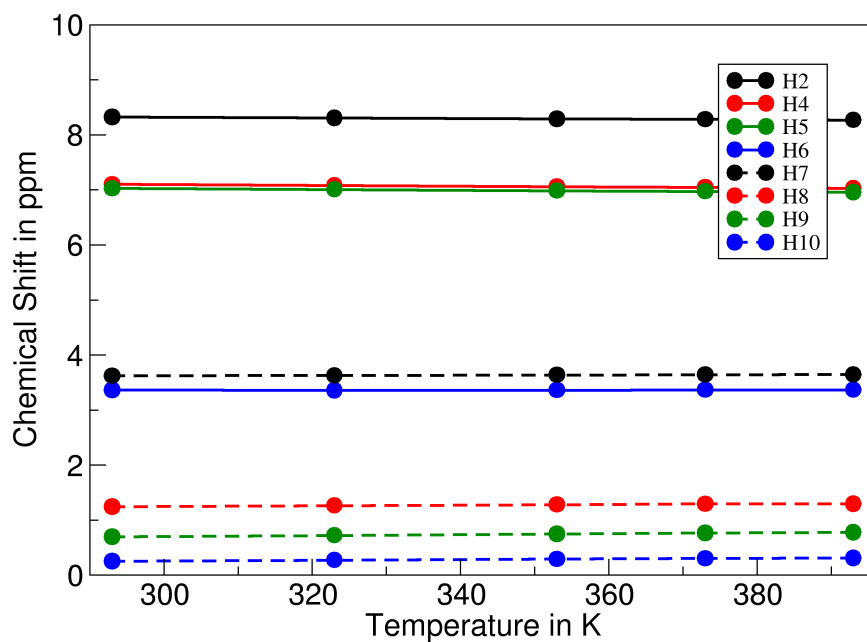


Figure 41: Chemical Shifts of the hydrogen atoms in the pure $[C_4C_1Im][OTf]$ at different temperatures.

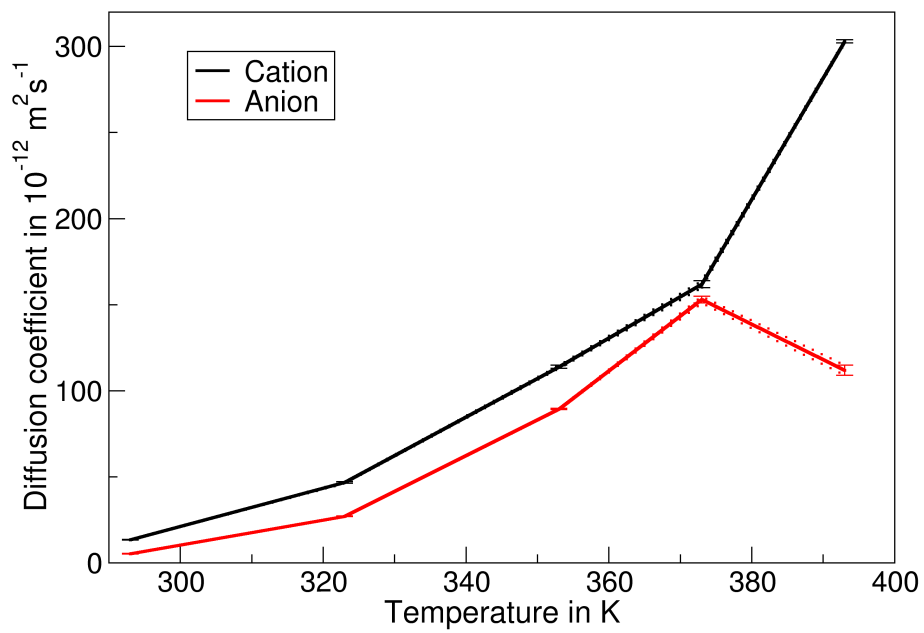


Figure 42: Diffusion coefficients in the pure $[\text{C}_4\text{C}_1\text{Im}][\text{OTf}]$ at different temperatures.

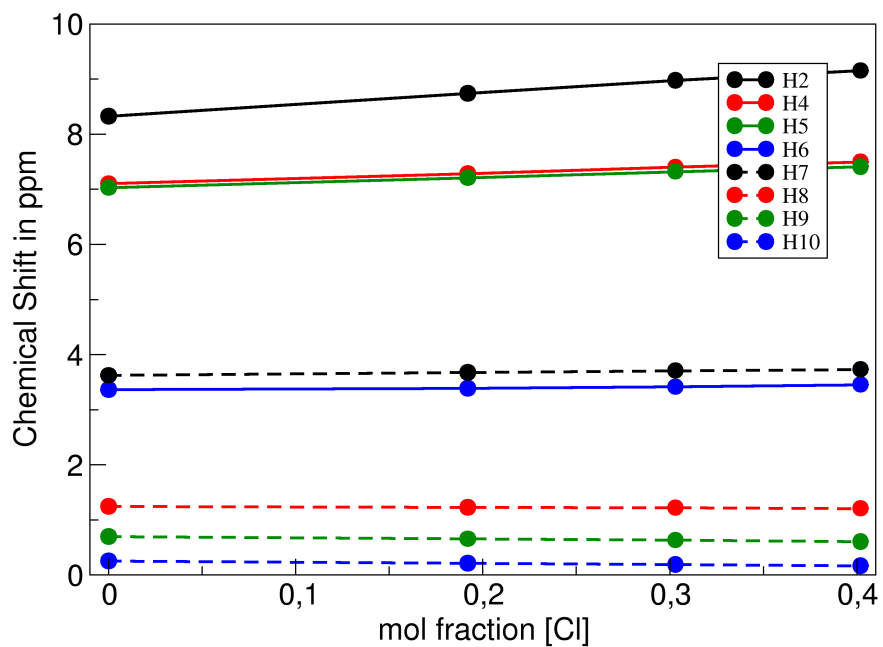


Figure 43: Chemical Shifts of the hydrogen atoms in the ionic liquid mixtures.

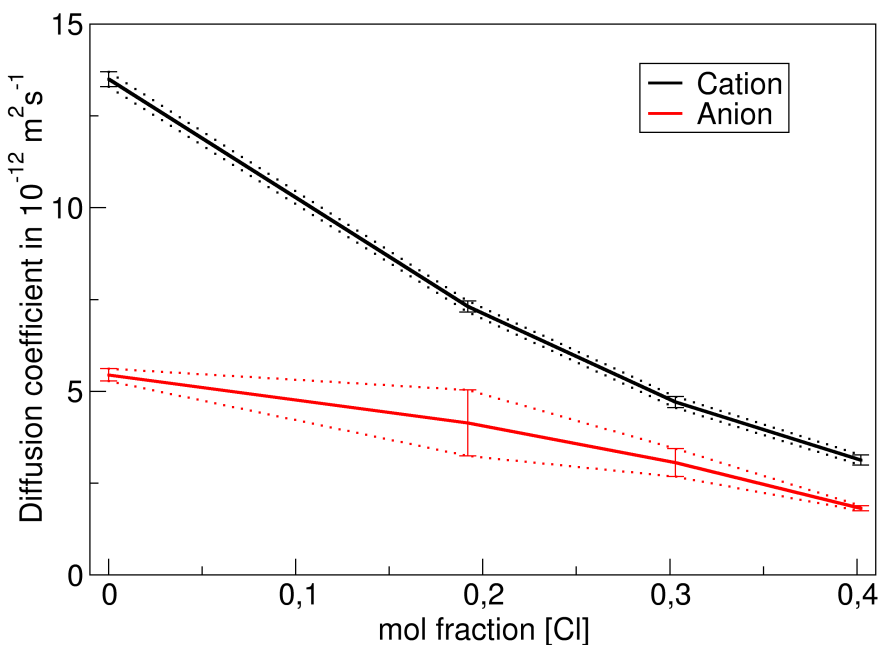


Figure 44: Diffusion coefficients in the ionic liquid mixtures.

References

- [1] W. L. Jorgensen, D. S. Maxwell and J. Tirado-Rives, *J. Am. Chem. Soc*, 1996, **118**, 11225–11236.
- [2] J. N. Canongia Lopes and A. A. Pádua, *J. Phys. Chem. B*, 2006, **110**, 19586–19592.
- [3] J. N. Canongia Lopes and A. A. Pádua, *J. Phys. Chem. B*, 2004, **108**, 16893–16898.
- [4] A. Dequidt, J. Devémy and A. A. H. Pádua, *J. Chem. Inf. Model.*, 2016, **56**, 260–268.
- [5] C. E. S. Bernardes, K. Shimizu, J. N. C. Lopes, P. Marquetand, E. Heid, O. Steinhauser and C. Schroder, *Phys. Chem. Chem. Phys.*, 2016, **18**, 1665–1670.
- [6] G. Lamoureux and B. Roux, *J. Phys. Chem. B*, 2006, **110**, 3308–3322.
- [7] H. Berendsen, J. Grigera and T. Straatsma, *J. Phys. Chem.*, 1987, **91**, 6269–6271.
- [8] H. A. Lorentz, *Ann. Phys.*, 1881, **248**, 127–136.

- [9] D. Berthelot, *Compt. Rendus*, 1898, **126**, 1703–1855.
- [10] R. W. Hockney and J. W. Eastwood, *Computer simulation using particles*, CRC Press, 1988.
- [11] S. Plimpton, *J. Comp. Phys.*, 1995, **117**, 1–19.
- [12] L. Martínez, R. Andrade, E. G. Birgin and J. M. Martínez, *J. Comp. Chem.*, 2009, **30**, 2157–2164.
- [13] S. Nosé, *J. Chem. Phys.*, 1984, **81**, 511–519.
- [14] S. Nosé, *Mol. Phys.*, 1984, **52**, 255–268.
- [15] G. J. Martyna, M. L. Klein and M. Tuckerman, *J. Chem. Phys.*, 1992, **97**, 2635–2643.
- [16] R. L. Gardas, M. G. Freire, P. J. Carvalho, I. M. Marrucho, I. Fonseca, A. G. Ferreira and J. A. Coutinho, *J. Chem. Eng. Data*, 2007, **52**, 80–88.
- [17] M. Shamsipur, A. A. M. Beigi, M. Teymouri, S. M. Pourmortazavi and M. Irandoost, *J. Mol. Liq.*, 2010, **157**, 43–50.
- [18] M.-L. Ge, R.-S. Zhao, Y.-F. Yi, Q. Zhang and L. S. Wang, *J. Chem. Eng. Data*, 2008, **53(10)**, 2408–2411.
- [19] M. T. Clough, C. R. Crick, J. Gräsvik, P. A. Hunt, H. Niedermeyer, T. Welton and O. P. Whitaker, *Chem. Sci.*, 2015, **6**, 1101–1114.
- [20] M. Brehm and B. Kirchner, *J. Chem. Inf. Model.*, 2011, **51**, 2007–2023.
- [21] T. Williams, C. Kelley, H. Bröker, J. Campbell, R. Cunningham, D. Denholm, E. Elber, R. Fearick, C. Grammes and L. Hart, *URL <http://www.gnuplot.info>*.
- [22] P. Turner, *Center for Coastal and Land-Margin Research, Oregon Graduate Institute of Science and Technology, Beaverton, OR*, 2005.
- [23] A. Khintchine, *Math. Ann.*, 1934, **109**, 604–615.
- [24] N. Wiener, *Acta math.*, 1930, **55**, 117–258.
- [25] R. L. Gardas and J. A. Coutinho, *AIChE J.*, 2009, **55**, 1274–1290.
- [26] G. McHale, C. Hardacre, R. Ge, N. Doy, R. W. K. Allen, J. M. MacInnes, M. R. Brown and M. I. Newton, *Anal. Chem.*, 2008, **80**, 5806–5811.
- [27] J.-M. Andanson, X. Meng, M. Traikia and P. Husson, *J. Chem. Thermodyn.*, 2016, **94**, 169–176.
- [28] M. L. S. Batista, L. I. N. Tome, C. M. S. S. Neves, J. R. B. Gomes and J. A. P. Coutinho, *J. Mol. Liq.*, 2014, **192**, 26–31.

- [29] M. Tsamba, S. Sarraute, M. Traikia and P. Husson, *J. Chem. Eng. Data*, 2014, **59(6)**, 1747–1754.
- [30] H. Tokuda, S. Tsuzuki, M. A. B. H. Susan, K. Hayamizu and M. Watanabe, *J. Phys. Chem. B*, 2006, **110(39)**, 19593–19600.
- [31] E. O. Stejskal and J. E. Tanner, *J. Chem. Phys.*, 1965, **42**, 288–292.